Statin-mediated reduction in mitochondrial cholesterol primes an anti-inflammatory response in macrophages by upregulating JMJD3

Zeina Salloum[1], Kristin Dauner[1], Neha Verma[1], John D. Zhang[1], Kiran Nakka[2], David Valdivieso-González[3,4], Víctor Almendro-Vedia[3,4], Jeffery McDonald[5], Alexander Sorisky[1,7], Iván López-Montero[3,4], F. Jeffrey Dilworth[2,6], Xiaohui Zha[1,7,8]

[1]Chronic Disease Program, Ottawa Hospital Research Institute, Ottawa, ON, K1H 8L6, Canada.

[2]Sprott Center for Stem Cell Research, Regenerative Medicine Program, Ottawa Hospital Research Institute, Ottawa, ON K1H 8L6, Canada.

[3]Departamento Química Física, Universidad Complutense de Madrid, Avda. Complutense s/n, 28040, Madrid, Spain.

[4]Instituto de Investigación Biomédica Hospital Doce de Octubre (imas12), Avenida de Córdoba s/n, 28041, Madrid, Spain.

[5]Department of Molecular Genetics, The University of Texas Southwestern Medical Center, Dallas, TX, USA.

[6]Department of Cellular and Molecular Medicine, University of Ottawa, Ottawa, ON K1H 8L6, Canada.

[7]Departments of Medicine and of Biochemistry, Microbiology & Immunology, University of Ottawa, Ottawa, ON, K1H 8L6, Canada.

[8]Email: xzha@ohri.ca

Classifications: *Biological Sciences*

Key words: *cholesterol, statin, methyl-β-cyclodextrin, mitochondria, JMJD3, bone-marrow derived macrophages, LPS, IL-4*

Abstract

Cholesterol plays an important role in regulating macrophage inflammatory responses, but the mechanism is poorly understood. Here we show that reducing cholesterol in macrophages by statins upregulates JMJD3, a H3K27me3 demethylase. We provide evidence that this upregulation involves altered mitochondrial function, particularly the ATP synthase in the inner mitochondrial membrane (IMM). ATP synthase is suppressed by statin due to reduced cholesterol levels in IMM. This promotes JMJD3 expression. We also demonstrate that reducing cholesterol in macrophages alters the epigenetic configuration or epigenome. When macrophages are classically activated (M1), statin treatment suppresses the pro-inflammatory phenotype while enhancing anti-inflammatory IL-10 expression. On the other hand, when macrophages are alternatively activated (M2), statins promote the expression of Arg1, Ym1, and Mrc1. The enhanced expression of these anti-inflammatory factors correlates with H3K27me3 removal by statins in resting macrophages prior to activation. Lastly, we provide evidence that JMJD3 demethylase activity is necessary for cholesterol to modulate M1 and M2 activation in macrophages. We conclude that upregulation of JMJD3 in macrophages plays a key role in the anti-inflammatory effects of statins.

Significance Statement

In addition to lowering the plasma LDL, statins exert a well-documented anti-inflammatory effect clinically, though the mechanism is unknown. We show here that, by decreasing cellular cholesterol content, statins reduce cholesterol in the IMM to upregulates JMJD3, which is essential for anti-inflammatory functions in macrophages. This novel mechanism may potentially operate *in vivo*. Bone-marrow derived cells, including macrophages, are highly proliferating and require plasma LDL and cholesterol biosynthesis to provide cholesterol for new membrane production. By lowering the plasma LDL and inhibiting HMG-CoA reductase, statin therapy could generate macrophages with relatively less cholesterol in membranes, including the IMM, thereby promoting JMJD3 expression and anti-inflammatory function. This could contribute at least in part to observed anti-inflammatory effects of statins in human population.

Main Text

Many chronic diseases including atherosclerosis are associated with a low-grade level of inflammation (1). In atherosclerosis, macrophages are overloaded with cholesterol and are inflamed, which causes lesion formation (2). Statins reduce circulating cholesterol and also reduce inflammation, but the mechanism for the anti-inflammatory effect is not clear (3). Previously, we and others have observed that the level of cholesterol in resting macrophages, i.e., prior to stimulation, directly correlates with their pattern of inflammatory activation (4-6). For instance, when encountering lipopolysaccharides (LPS), cholesterol-rich macrophages release more inflammatory cytokines, such as TNF-α, IL-6, and IL12p40, and less anti-inflammatory cytokine IL-10, relative to control macrophages. Conversely, macrophages with reduced cholesterol, such as these expressing ABCA1/G1, express fewer inflammatory cytokines and more IL-10 upon identical LPS exposure (4-6). Noticeably, the effect of cholesterol on macrophage inflammation is similar across multiple stimuli, including ligands to TLR2, 3, 4 et al (5). Macrophages are known to activate several hundred genes immediately upon immune stimuli, in order to mount a vigorous defence against pathogens (7). This is achieved by employing limited number of signal-dependent transcription factors, such as NF-κB, on already "open" (or partially open) genome regions (8). Such a genomic configuration or epigenome is established by both lineage-determining transcription factors and metabolic/environmental cues, including from previous exposures (8, 9). This allows macrophages to fine-tune gene expression profiles upon future stimulation (10, 11). We speculate that cholesterol levels in macrophages may directly impact the epigenome, which then influences the macrophage phenotype upon subsequent activation.

Results

To test whether cholesterol levels alone can influence epigenetic modifications in macrophages, we first treated RAW macrophages with statins[*] for 2 days, which reduces cellular cholesterol by about 30% (4, 12). We also used 1 h methyl-β-cyclodextrin (MCD) treatment to acutely reduce cholesterol by a similar amount (4). This was aimed to, first, verify the cholesterol specificity of statins' effects and, secondly, provide a 1 h-regimen for potential inhibitor studies. RNA-seq was performed at the end of statin or MCD treatments. Macrophages treated with statins upregulated 672 genes (log2>1), whereas MCD increased the expression of 51 genes (log2>1). There were 40 genes affected by both. We verified the upregulation of several genes among these 40 using qPCR in MCD-treated macrophages (Fig. 1A, *a*). We noted JMJD3, a major histone H3K27me3 demethylase (13), was upregulated by both statins and MCD (Fig. 1A, *b*). JMJD3 is a known NF-κB target (14). Indeed, using two structurally unrelated NF-κB inhibitors, we observed that the upregulation of JMJD3 is dependent on NF-κB activity (Fig. 1A, c). We further confirmed that JMJD3 protein level is increased (Fig. 1A, *d*) and that the level of H3K27me3, the substrate of JMJD3, is reciprocally decreased in macrophages with reduced cholesterol by MCD (Fig. 1A, *h*).

[*] Lovastatatin, compactin, simvastatin and pravastatin were used exchangeably throughout the study without significant differences in results.

The level of phosphorylated Creb (pCreb) is used as indicator of effective cholesterol reduction (4). Similar results were seen in macrophages treated with statins (Supplementary Fig. 1). Significantly, we observed identical effects cholesterol reduction in mouse bone marrow-derived macrophages (BMDM): JMJD3 is upregulated in BMDMs by statins or MCD in a NF-κB-dependent manner (Fig. 1B, *a & b*). Lastly, to verify the specificity of cholesterol in JMJD3 upregulation, we used MCD/cholesterol complex to replenish cellular cholesterol in MCD-treated BMDMs. This reversed the JMJD3 upregulation by MCD in BMDMs (Fig. 1 C). We conclude that statins upregulate JMJD3 in macrophages through cholesterol reduction and NF-κB activation.

To explore the mechanisms, we analyzed the major TFs responsible for statin- or MCD-induced genes in RNA-seq, using a database of mouse transcriptional regulatory networks (15) embedded in Metascape (16). Analysis of promoter sequences of the differentially expressed genes identified Nfkb1 as the top regulator of genes that enhanced their expression upon treatment with either statins or MCD (Fig. 2A, *a & b*). This is confirmed by elevated NF-κB activity in MCD- or statins-treated macrophages (Fig. 2B, *a & b*), using RAW-Blue™ cells containing NF-κB reporter (17). Furthermore, two known NF-κB target genes, namely IL-1β and TNF-α, are upregulated by MCD and statins, respectively (Fig. 2B, *c & d*). In addition, blocking NF-κB function by two inhibitors prevented the upregulation of IL-1β and TNF-α by MCD (Fig. 2B, *e & f*), confirming the role for NF-κB in modulating the effects of cholesterol depletion (Fig. 2A). Lastly, to understand the scope of NF-κB activation by statins or MCD, we compared the magnitude of IL-1β and TNF-α expression by statin or MCD with these by LPS. The effect of statins or MCD is small: IL-1β and TNF-α expressions by statin/MCD are less than 1% of these stimulated by LPS (Supplementary Fig. 2). This suggests that statin/MCD activate NF-κB to serve different purposes than to launch acute inflammation responses.

We next studied potential mechanisms by which statin/MCD might activate NF-κB. In recent years, it has become evident that NF-κB can be activated when a metabolic shift occurs from oxidative phosphorylation (OXPHOS) in the mitochondria to glycolysis in the cytoplasm (18, 19). We therefore investigated whether statin/MCD modulates OXPHOS in macrophage to activate NF-κB. Using the extracellular flux analyzer (Seahorse), we found that 1 h MCD treatment of BMDMs decreases overall resting mitochondrial oxygen consumption rate (OCR) (Fig. 3A, *a*). Moreover, this decrease is entirely due to the inhibition of the ATP synthase (Fig. 3A, *b*), which is embedded in the inner mitochondrial membrane (IMM). The maximal respiration remains unchanged by MCD (Fig. 3A, *c*). Statin treatment similarly decreases overall resting mitochondrial OCR (Fig. 3B, *a*) and that of ATP synthase (Fig. 3B, *b*). However, statin also lowers the maximal respirations (Fig. 3B, *c*), suggesting a broader influence on the mitochondria than MCD, possibly due to the 2-day treatment period required for the statins. The OCRs in RAW macrophages are identically affected by statin/MCD (Supplementary Fig. 3). Thus, statin or MCD suppresses mitochondria respiration and inhibits the ATP synthase in IMM in macrophages.

We asked how statin/MCD might influence mitochondria respiration, particularly a component of electron transport chain, namely the ATP synthase, in the IMM. In mammalian cells, the majority of cholesterol is in the plasma membrane. However, all intracellular membranes,

including those in the mitochondria, also contain cholesterol (20). Cholesterol distributions among cellular membranes is governed by a dynamic steady state (21); reduction in total cellular cholesterol content, such as by statin or MCD, would decrease cholesterol content in all membranes, including those in the mitochondria (22). Levels of IMM cholesterol can be accessed by the activity of an IMM enzyme, sterol 27-hydroxylase (*CYP27A1*). It catalyzes the conversion of cholesterol to 27-hydroxycholesterol as a function of cholesterol availability in the IMM (23). The amount of 27-hydroxycholesterol in macrophages thus directly reflects cholesterol levels in the IMM, if *CYP27A1* remains constant (22). We found that *CYP27A1* levels are significantly reduced by 2-day statin treatment (Supplementary 4) but remain steady after 1 h MCD treatment (Fig. 4A). We thus analyzed 27-hydroxycholesterol contents by mass spectrometry on MCD-treated macrophages to assess the cholesterol levels in IMM. We find that cellular 27-hydroxycholesterol content is decreased in a dose-dependent manner after a 1 h MCD treatment (Fig. 4B), demonstrating reduced cholesterol levels in IMM by MCD treatment. Statins decrease total cholesterol contents in macrophages in a manner similar to MCD (4), which would be expected to lower cholesterol levels in all cellular membranes including IMM, even though the assay could not be applied due to the changes in *CYP27A1* expression.

To understand precisely how cholesterol levels in IMM might influence ATP synthase functions, we turned to an *in-vitro* membrane system composed of inner membrane vesicles from *Escherichia coli (*IMVs) (24). *E. coli* inner membrane shares common features with ones in mammalian cells (25), including ATP synthase functions (26), but lacks cholesterol or any other sterol derivative in their lipid composition (27). Various levels of cholesterol could be incorporated into the IMVs to access the impact of cholesterol (28). With this system, we observed that the activity of the ATP synthase, both in synthesis and hydrolysis mode, is highly sensitive to cholesterol concentrations in the membrane: the highest activity is found in IMV with membrane containing 7% cholesterol; decreasing or increasing cholesterol from 7% cholesterol supresses ATP synthase activities (Fig. 4C). The steady-state IMM cholesterol level in mammalian cells is about 5% (29). If MCD reduces cholesterol in IMM, as we show above (Fig. 4 B), ATP synthase activity should be suppressed, as we have seen in OCR (Fig. 3 A, b). Therefore, the *in-vitro* experimental model is consistent with the notion that MCD lowers cholesterol in the IMM, which suppresses ATP synthase activity.

We next studied potential role of suppressed ATP synthase in NF-κB activation and JMJD3 upregulation. ATP synthase in IMM uses proton flow from the inner space to the matrix to generate ATP (Fig. 5A, a). As shown by extracellular flux analysis (Fig. 3), statin/MCD suppresses the activities of ATP synthase. This would lead to fewer protons flowing down from the inner space into the matrix and, consequently, more protons would be retained in the inner space in statin/MCD treated macrophages (Fig. 5A, *b*), which could serve as the source to activate NF-κB (30). We tested this possibility using carbonyl cyanide m-chlorophenyl hydrazine (CCCP), a mitochondrial proton ionophore that prevents proton buildup in the inner space (31) (Fig. 5A, *c*). Indeed, in the presence of CCCP, MCD fails to activate NF-κB (Fig. 5B, *a*). CCCP also abolishes JMJD3 upregulation by MCD in both RAW macrophages and BMDMs (Fig. 5B, *b* & *c*). In addition, CCCP prevents MCD from upregulating IL-1β (Fig. 5 B, *d*). Moreover, another structurally unrelated mitochondrion proton ionophore BAM15 (32) similarly abolished MCD induced IL-1β

and JMJD3 expression (Supplementary Fig. 5). We conclude that reducing cholesterol in macrophages suppresses ATP synthetase activity in the IMM, which activates NF-κB and upregulates JMJD3.

JMJD3 primarily functions to demethylate H3K27me3, an abundant epigenetic mark associated with transcriptional repression (33). The upregulation of JMJD3 by statin/MCD decreases H3K27me3, which should have an impact on the epigenome. We performed the assay for transposase-accessible chromatin with sequencing (ATAC-seq) and compared the transposase accessibility with or without MCD. We observed that MCD significantly altered the epigenome: 2791 genes were more accessible (red), whereas another 1000 genes were less accessible (grey) (Fig. 6A). The result suggests that multiple epigenetic modifying factors, in addition to JMJD3, are activated by MCD treatment. This new epigenome could poise resting macrophages for alternative inflammatory responses. We therefore tested MCD or statin effect on macrophages stimulated with LPS, i.e. classically activated (M1) or IL-4, alternatively activated (M2).

Statin-treated RAW macrophages were stimulated by LPS and RNA-seq was performed. As expected, LPS activated a large number of genes. Among these, a group of genes, which includes TNF-α, is expressed less in statin-treated macrophages (Fig. 6B, *a*). GO analysis of this group reveals predominately pro-inflammatory nature (Fig. 6B, b). At the same time, statins enhance LPS-stimulated expression of IL-10 (Fig. 6B, c). A similar pattern is seen in MCD-treated macrophages (Supplementary Fig. 6). We next examined the potential contribution of JMJD3 to this effect, using the ratio of IL-10/TNF-α as indicator, as we have established previously (4). JMJD3 belongs to the JmjC demethylase family that requires α-ketoglutarate (α-KG) as co-factor to demethylate histone (34). Noticeably, JMJD3 (KDB6b) is the only member of the JmjC family upregulated by MCD in macrophages and, importantly, the expression of closely related UTX (KDB6a) is not changed by cholesterol reduction (Fig. 6C, a). This presented an opportunity to specifically probe the involvement of JMJD3 demethylation activity in suppressing TNF-α and raising IL-10 expression by MCD. JMJD3 expression is increased with MCD concentrations (Fig. 6C, *b*). When subsequently stimulated by LPS, MCD-treated macrophages dose-dependently express less TNF-α, but more IL-10: the ratio of IL-10/TNF-α rises with MCD concentrations (Fig. 6C, *c*, light bars). However, if glutamine, the precursor of α-KG (34), is absent in the medium, there is little change in the ratio of IL-10/TNF-α (Fig. 6A, *c*, black bars), regardless of MCD concentration. Furthermore, if JMJD3 is inhibited by a specific inhibitor GSKj4 (35), the ratio of IL-10/TNF-α also failed to rise by MCD (Fig. 6C, *d*). Statin-treated macrophages primarily upregulate JMJD3, not UTX (Supplementary Fig. 7), consistent with the role of JMJD3 in modulating LPS responses.

Statin-treated BMDMs similarly modify their response to LPS as above. When stimulated by LPS, statin-treated BMDMs express less TNF-α, IL-1b, IL-6 and IL-12, compared to control, and, at the same time, express more IL-10 (Fig. 7A), thereby raising the ratio of IL-10/TNF-α as above. Importantly, this rise IL-10/TNF-α ratio is dependent on glutamine: IL-10/TNF-α fails to rise by MCD in the absence of glutamine (Fig 7B). Together with results from RAW macrophages (Fig. 6), we conclude that, in response to LPS stimulation, statin or MCD suppresses proinflammatory

phenotype and enhances the expression of IL-10 in macrophages. This modulation depends on JMJD3 demethylase activity.

We next stimulated statin-treated BMDMs with IL-4. The expression of Arg1, Ym1, and Mrc1 is enhanced by statin, relative to untreated controls (Fig. 7*C*). We then tested if enhanced M2 gene expression by cholesterol reduction relies on JMJD3 enzymatic activity. We observed that glutamine is necessary for MCD to boost IL4-targeted Arg1 (Fig. 7D). Thus, statin/MCD promote anti-inflammatory M2 activation in macrophages, and this effect relies on JMJD3 demethylase activities.

Lastely, chromatin immunoprecipitation (ChIP) using antibody against H3K27me3 was performed on statin-treated BMDMs. We observed that statins reduce H3K27me3 on IL-4 target genes in resting macrophages (Fig. 7E), consistent with their enhanced expression upon IL4 stimulation (Fig. 7*C*). In addition, statins also reduce H3K27me3 on IL-10 (Fig. 7*E*, *desert* as input control), agreeing with its upregulation in LPS-stimulated macrophages above (Fig. 7*B*). We conclude that reducing cholesterol by statins in macrophages results in phenotypical changes in their immune responses; both M1 and M2 activation shifts toward a more anti-inflammatory phenotype in a JMJD3-dependent manner.

Discussion

In this study, we identify a mechanism by which reducing cholesterol in macrophages with statin/MCD upregulates JMJD3 through suppressing mitochondria respiration. Cholesterol reduction also modifies the epigenome in macrophages. Upon subsequent activation by either M1 or M2 stimuli, statin-treated macrophages are phenotypically more anti-inflammatory.

We provide evidence that this is likely due to removing H3K27me3, a repressive mark, by JMJD3. Macrophages have two H3K27me3 demethylases, UTX and JMJD3. Only JMJD3 is upregulated by statin or MCD. We speculate that, by removing H3K27me3 from Arg1, Yam1, and Mrc1, JMJD3 poises these genes to promote the expression upon IL-4 activation in statin treated macrophages. On the other hand, statin primarily suppresses a large group of proinflammatory genes activated by LPS, which could not directly be attributed to JMJD3. However, H3K27me3 is removed from IL-10 by statin, which is correlated with enhanced IL-10 expression by LPS stimulation. Likely, the upregulation of IL-10 is instrumental for the suppression of proinflammatory phenotype in LPS activation. Indeed, recent studies show that endogenously produced IL-10, through autocrine/paracrine mechanisms, modulates mitochondria respiration to inhibit cellular events, such as glycolysis and mTORC1. This suppresses the expression of proinflammatory genes (36, 37). The elevated IL-10 expression in statin/MCD treated macrophages could play similar role to suppress the proinflammatory phenotypes.

We also document here that reducing macrophage cholesterol alters the epigenome, concurrent with JMJD3 upregulation. Removing H3K27me3 by JMJD3 would open certain genome regions, for example on Arg1, Yam1, Mrc1 and IL-10, and contribute to the changes in the epigenome seen in ATCA-seq. However, the changes we observed are much more profound, indicating that

other modifiers, in addition to JMJD3, are activated by cholesterol reduction. Future studies will be required to identify these modifiers. Nevertheless, our results support the notion that JMJD3 is perhaps most relevant to inflammatory activation, particularly these influenced by statins. First of all, only JMJD3, among the members of the JmjC demethylase family, is upregulated by statin or MCD. UTX, also a H3K27me3 demethylase, is not altered by statin or MCD. Secondly, the JmjC demethylase family members require glutamine, the source of a-ketoglutarate, for demethylation. Since JMJD3 is the only upregulated demethylase, glutamine could be used to specifically probe JMJD3 demethylation function in macrophages M1/M2 activation. Glutamine is indeed sufficient and necessary for MCD to modulate both LPS and IL-4 activation. Thirdly, GSKj4, the inhibitor for H3K27me3 demethylase, abolishes the MCD effect. Thus, the upregulation of JMJD3 by statin/MCD likely contributes to poise the epigenome in resting macrophages, which controls the subsequent inflammatory response to LPS or IL-4.

Our results here support the notion that the epigenome in macrophages is poised for inflammatory activation (38). This also agrees with previous studies where cholesterol reduction decreases proinflammatory response to multiple stimuli against various TLRs (5). We have focused on classically activated (M1) and alternatively activated (M2) phenotypes, two extremes of inflammatory activation in macrophages. However, their mechanistic exploration could provide a starting point, as macrophages likely encounter a wide range of stimuli within a continuum between M1 and M2. The poised epigenome, i.e. in resting macrophages prior to activation, may serve as an initial blueprint that impact on activated inflammatory responses. In addition, the inflammation processes are thought to initially engage the M1 phenotype to fight pathogens and then to gradually obtain M2 phenotype to restrain excessive damage and restore tissue homeostasis (11).

Another novel finding here is that cholesterol directly controls mitochondria respiration. Except for specialized cell types (i.e. steroidogenic cells), the mitochondrial cholesterol in mammalian cells is an integral part of cellular cholesterol and, as such, varies with cellular cholesterol through a dynamic steady state (20). Our study here for the first time implicates the mitochondria membrane as a locus for the cellular cholesterol level to control metabolic processes and gene expression. This is somewhat analogous to the regulation of SREBP pathways by the cellular cholesterol level through the ER membrane (39). It places the mitochondria at the center of essential cellular regulations, far beyond the traditionally called powerhouse to produce ATP (40). The full scope of this regulation remains to be seen, and more work will be required to determine if it is applicable to other cell types.

Lastly, our study addresses the anti-inflammation functions of statins. Statins are clinically used to lower the plasma cholesterol, mainly LDL. As specific inhibitors of the HMG-CoA reductase, statins prevent cholesterol biosynthesis, which in the liver upregulates hepatic LDL receptors to enhance LDL clearance. Statins are also known for their anti-inflammatory functions, through unknown mechanisms (41). We speculate that statins may reduce cholesterol contents in peripheral cells, particularly those that are highly proliferative, such as bone-narrow derived cells. These cells have a high demand for cholesterol to generate new membranes, which is normally supplied by both uptake of plasma LDL and cholesterol biosynthesis. Statins could limit

cholesterol supply by lowering circulating LDL and preventing biosynthesis. Indeed, studies show that statins can reach circulating macrophages in sufficient concentration to inhibit HMG-CoA *in vivo* (42). Given our data here, it is plausible that, by limiting cholesterol levels in bone-marrow derived cells, including monocytes/macrophages, statins could promote anti-inflammatory functions in macrophages. This could at least partially account for statin's anti-inflammatory functions observed in human population (41).

Data availability

GSE196187, GSE196188, GSE196189

Acknowledgements
This work was supported by a grant (grant-in-aid) from Heart and Stroke Foundation of Canada (HSFC), G-19-0026359 and a grant from Canadian Institute of Health Research (CIHR), PJT-180504. This work was also supported in part by the TECNOLOGÍAS 2018 program funded by the Regional Government of Madrid (Grant S2018/BAA-4403 SINOXPHOS-CM, to ILM) and by a grant from NIH (HL020948, to JGM). We thank Dr. T. Lagace for reagents, and Dr. M. Harper for access to use the XFe96 Seahorse Extracellular Flux Analyzer. We also knowledge the technical assistance of H. Bandukwala and E. S. Qamsar.

Author contributions

Conceptualization - ZS, XZ
Data acquisition - ZS, NV, KD, KN, JDZ, DVG, VAV, JM
Data analysis - ZS, NV, DVG, VAV, JM, FJD, XZ
Supervision - XZ, FJD, ILM
Writing – ZS, XZ, AS, FJD, ILM

References

1. Tabas I, Glass CK. Anti-inflammatory therapy in chronic disease: challenges and opportunities. Science. 2013 Jan 11;339(6116):166-72.
2. Tabas I, Lichtman AH. Monocyte-Macrophages and T Cells in Atherosclerosis. Immunity. 2017 Oct 17;47(4):621-634.
3. Libby P. Inflammation in Atherosclerosis-No Longer a Theory. Clin Chem. 2021 Jan 8;67(1):131-142.
4. Ma L, Dong F, Zaid M, Kumar A, Zha X. ABCA1 protein enhances Toll-like receptor 4 (TLR4)-stimulated interleukin-10 (IL-10) secretion through protein kinase A (PKA) activation. J Biol Chem. 2012 Nov 23;287(48):40502-12.
5. Yvan-Charvet L, Welch C, Pagler TA, Ranalletta M, Lamkanfi M, Han S, Ishibashi M, Li R, Wang N, Tall AR. Increased inflammatory gene expression in ABC transporter-deficient macrophages: free cholesterol accumulation, increased signaling via toll-like receptors, and neutrophil infiltration of atherosclerotic lesions. Circulation. 2008 Oct 28;118(18):1837-47.
6. Zhu X, Lee JY, Timmins JM, Brown JM, Boudyguina E, Mulya A, Gebre AK, Willingham MC, Hiltbold EM, Mishra N, Maeda N, Parks JS. Increased cellular free cholesterol in macrophage-specific Abca1 knock-out mice enhances pro-inflammatory response of macrophages. J Biol Chem. 2008 Aug 22;283(34):22930-41.
7. Raetz CR, Garrett TA, Reynolds CM, Shaw WA, Moore JD, Smith DC Jr, Ribeiro AA, Murphy RC, Ulevitch RJ, Fearns C, Reichart D, Glass CK, Benner C, Subramaniam S, Harkewicz R, Bowers-Gentry RC, Buczynski MW, Cooper JA, Deems RA, Dennis EA. Kdo2-Lipid A of Escherichia coli, a defined endotoxin that activates macrophages via TLR-4. J Lipid Res. 2006 May;47(5):1097-111.
8. Link VM, Gosselin D, Glass CK. Mechanisms Underlying the Selection and Function of Macrophage-Specific Enhancers. Cold Spring Harb Symp Quant Biol. 2015; 80:213-21.
9. Troutman TD, Kofman E, Glass CK. Exploiting dynamic enhancer landscapes to decode macrophage and microglia phenotypes in health and disease. Mol Cell. 2021 Oct 7;81(19):3888-3903.
10. Spann NJ, Garmire LX, McDonald JG, Myers DS, Milne SB, Shibata N, Reichart D, Fox JN, Shaked I, Heudobler D, Raetz CR, Wang EW, Kelly SL, Sullards MC, Murphy RC, Merrill AH Jr, Brown HA, Dennis EA, Li AC, Ley K, Tsimikas S, Fahy E, Subramaniam S, Quehenberger O, Russell DW, Glass CK. Regulated accumulation of desmosterol integrates macrophage lipid metabolism and inflammatory responses. Cell. 2012 Sep 28;151(1):138-52
11. Ivashkiv LB. Epigenetic regulation of macrophage polarization and function. Trends Immunol. 2013 May;34(5):216-23.
12. Mayor S, Sabharanjak S, Maxfield FR. Cholesterol-dependent retention of GPI-anchored proteins in endosomes. EMBO J. 1998 Aug 17;17(16):4626-38.
13. De Santa F, Totaro MG, Prosperini E, Notarbartolo S, Testa G, Natoli G. The histone H3 lysine-27 demethylase Jmjd3 links inflammation to inhibition of polycomb-mediated gene silencing. Cell. 2007 Sep 21;130(6):1083-94
14. De Santa F, Narang V, Yap ZH, Tusi BK, Burgold T, Austenaa L, Bucci G, Caganova M, Notarbartolo S, Casola S, Testa G, Sung WK, Wei CL, Natoli G. Jmjd3 contributes to the

control of gene expression in LPS-activated macrophages. EMBO J. 2009 Nov 4;28(21):3341-52.
15. Han H, Cho JW, Lee S, Yun A, Kim H, Bae D, Yang S, Kim CY, Lee M, Kim E, Lee S, Kang B, Jeong D, Kim Y, Jeon HN, Jung H, Nam S, Chung M, Kim JH, Lee I. TRRUST v2: an expanded reference database of human and mouse transcriptional regulatory interactions. Nucleic Acids Res. 2018 Jan 4;46(D1):D380-D386.
16. Zhou Y, Zhou B, Pache L, Chang M, Khodabakhshi AH, Tanaseichuk O, Benner C, Chanda SK. Metascape provides a biologist-oriented resource for the analysis of systems-level datasets. Nat Commun. 2019 Apr 3;10(1):1523.
17. Hansen FC, Kalle-Brune M, van der Plas MJ, Strömdahl AC, Malmsten M, Mörgelin M, Schmidtchen A. The Thrombin-Derived Host Defense Peptide GKY25 Inhibits Endotoxin-Induced Responses through Interactions with Lipopolysaccharide and Macrophages/Monocytes. J Immunol. 2015 Jun 1;194(11):5397-406.
18. Tannahill GM, Curtis AM, Adamik J, Palsson-McDermott EM, McGettrick AF, Goel G, Frezza C, Bernard NJ, Kelly B, Foley NH, Zheng L, Gardet A, Tong Z, Jany SS, Corr SC, Haneklaus M, Caffrey BE, Pierce K, Walmsley S, Beasley FC, Cummins E, Nizet V, Whyte M, Taylor CT, Lin H, Masters SL, Gottlieb E, Kelly VP, Clish C, Auron PE, Xavier RJ, O'Neill LA. Succinate is an inflammatory signal that induces IL-1β through HIF-1α. Nature. 2013 Apr 11;496(7444):238-42.
19. Jha AK, Huang SC, Sergushichev A, Lampropoulou V, Ivanova Y, Loginicheva E, Chmielewski K, Stewart KM, Ashall J, Everts B, Pearce EJ, Driggers EM, Artyomov MN. Network integration of parallel metabolic and transcriptional data reveals metabolic modules that regulate macrophage polarization. Immunity. 2015 Mar 17;42(3):419-30.
20. Steck TL, Lange Y. Cell cholesterol homeostasis: mediation by active cholesterol. Trends Cell Biol. 2010 Nov;20(11):680-7. doi: 10.1016/j.tcb.2010.08.007. Epub 2010 Sep 16. PMID: 20843692; PMCID: PMC2967630.
21. Lange Y, Steck TL. Active cholesterol 20 years on. Traffic. 2020 Nov;21(11):662-674.
22. Lange Y, Steck TL, Ye J, Lanier MH, Molugu V, Ory D. Regulation of fibroblast mitochondrial 27-hydroxycholesterol production by active plasma membrane cholesterol. J Lipid Res. 2009 Sep;50(9):1881-8.
23. Li X, Hylemon P, Pandak WM, Ren S. Enzyme activity assay for cholesterol 27-hydroxylase in mitochondria. J Lipid Res. 2006 Jul;47(7):1507-12.
24. van der Does C, de Keyzer J, van der Laan M, Driessen AJ. Reconstitution of purified bacterial preprotein translocase in liposomes. Methods Enzymol. 2003;372:86-98.
25. Meyer A, Laverny G, Bernardi L, Charles AL, Alsaleh G, Pottecher J, Sibilia J, Geny B. Mitochondria: An Organelle of Bacterial Origin Controlling Inflammation. Front Immunol. 2018 Apr 19;9:536.
26. Nirody JA, Budin I, Rangamani P. ATP synthase: Evolution, energetics, and membrane interactions. J Gen Physiol. 2020 Nov 2;152(11):e201912475.
27. Sohlenkamp C, Geiger O. Bacterial membrane lipids: diversity in structures and pathways. FEMS Microbiol Rev. 2016 Jan;40(1):133-59.
28. Mahammad S. & Parmryd I. (2015) in *Methods in Membrane Lipids. Methods in Molecular Biology*, ed. D. IO (Humana Press, New York, NY).
29. Horvath SE, Daum G. Lipids of mitochondria. Prog Lipid Res. 2013 Oct;52(4):590-614.

30. Mills EL, Kelly B, Logan A, Costa ASH, Varma M, Bryant CE, Tourlomousis P, Däbritz JHM, Gottlieb E, Latorre I, Corr SC, McManus G, Ryan D, Jacobs HT, Szibor M, Xavier RJ, Braun T, Frezza C, Murphy MP, O'Neill LA. Succinate Dehydrogenase Supports Metabolic Repurposing of Mitochondria to Drive Inflammatory Macrophages. Cell. 2016 Oct 6;167(2):457-470.e13.
31. Lou PH, Hansen BS, Olsen PH, Tullin S, Murphy MP, Brand MD. Mitochondrial uncouplers with an extraordinary dynamic range. Biochem J. 2007 Oct 1;407(1):129-40.
32. Kenwood B.M., Weaver J.L., Bajwa A., Poon I.K., Byrne F.L., Murrow B.A. *et al.* (2013) Identification of a novel mitochondrial uncoupler that does not depolarize the plasma membrane. *Mol Metab.* **3,** 114-123.
33. Klose RJ, Kallin EM, Zhang Y. JmjC-domain-containing proteins and histone demethylation. Nat Rev Genet. 2006 Sep;7(9):715-27.
34. Liu PS, Wang H, Li X, Chao T, Teav T, Christen S, Di Conza G, Cheng WC, Chou CH, Vavakova M, Muret C, Debackere K, Mazzone M, Huang HD, Fendt SM, Ivanisevic J, Ho PC. α-ketoglutarate orchestrates macrophage activation through metabolic and epigenetic reprogramming. Nat Immunol. 2017 Sep;18(9):985-994.
35. Kruidenier L, Chung CW, Cheng Z, Liddle J, Che K, Joberty G, Bantscheff M, Bountra C, Bridges A, Diallo H, Eberhard D, Hutchinson S, Jones E, Katso R, Leveridge M, Mander PK, Mosley J, Ramirez-Molina C, Rowland P, Schofield CJ, Sheppard RJ, Smith JE, Swales C, Tanner R, Thomas P, Tumber A, Drewes G, Oppermann U, Patel DJ, Lee K, Wilson DM. A selective jumonji H3K27 demethylase inhibitor modulates the proinflammatory macrophage response. Nature. 2012 Aug 16;488(7411):404-8.
36. Ip WKE, Hoshi N, Shouval DS, Snapper S, Medzhitov R. Anti-inflammatory effect of IL-10 mediated by metabolic reprogramming of macrophages. Science. 2017 May 5;356(6337):513-519.
37. Dowling JK, Afzal R, Gearing LJ, Cervantes-Silva MP, Annett S, Davis GM, De Santi C, Assmann N, Dettmer K, Gough DJ, Bantug GR, Hamid FI, Nally FK, Duffy CP, Gorman AL, Liddicoat AM, Lavelle EC, Hess C, Oefner PJ, Finlay DK, Davey GP, Robson T, Curtis AM, Hertzog PJ, Williams BRG, McCoy CE. Mitochondrial arginase-2 is essential for IL-10 metabolic reprogramming of inflammatory macrophages. Nat Commun. 2021 Mar 5;12(1):1460.
38. Escoubet-Lozach L, Benner C, Kaikkonen MU, Lozach J, Heinz S, Spann NJ, Crotti A, Stender J, Ghisletti S, Reichart D, Cheng CS, Luna R, Ludka C, Sasik R, Garcia-Bassets I, Hoffmann A, Subramaniam S, Hardiman G, Rosenfeld MG, Glass CK. Mechanisms establishing TLR4-responsive activation states of inflammatory response genes. PLoS Genet. 2011 Dec;7(12):e1002401.
39. Brown MS, Goldstein JL. A proteolytic pathway that controls the cholesterol content of membranes, cells, and blood. Proc Natl Acad Sci U S A. 1999 Sep 28;96(20):11041-8.
40. Shen K, Pender CL, Bar-Ziv R, Zhang H, Wickham K, Willey E, Durieux J, Ahmad Q, Dillin A. Mitochondria as Cellular and Organismal Signaling Hubs. Annu Rev Cell Dev Biol. 2022 Oct 6;38:179-218.
41. Forrester JS, Libby P. The inflammation hypothesis and its potential relevance to statin therapy. Am J Cardiol. 2007 Mar 1;99(5):732-8.
42. Chow OA, von Köckritz-Blickwede M, Bright AT, Hensler ME, Zinkernagel AS, Cogen AL, Gallo RL, Monestier M, Wang Y, Glass CK, Nizet V. Statins enhance formation of phagocyte extracellular traps. Cell Host Microbe. 2010 Nov 18;8(5):445-54.

FIGURES LEGENDS

Figure 1. Satins upregulates the expression of JMJD3 in macrophages. (***A***) Statins and MCD upregulates JMJD3 in RAW 264.7 cells. (***a***) RT-qPCR of genes with or without MCD (5 mM; 1 h). ***(b)*** JMJD3 gene expression in MCD-, or statins- treated RAW 264.7 macrophages; ***(c)*** Effect of NF-kB inhibitors, MG-132 [5 µM] and BAY11-7082 [10 µM], on JMJD3 expression in MCD-treated RAW macrophages. ***(d)*** Western blotting of JMJD3 protein expression and ***(e)*** levels of H3K27Me3 in macrophages treated with 5 mM MCD (1h). The pCREB was used as internal control for cholesterol depletion and actin a loading control. (***B***) Statin upregulates JMJD3 in BMDMs. ***(a)*** JMJD3 gene expression in statins-treated BMDMs; ***(b)*** Effect of NF-kB inhibitors, MG-132 [5 µM] and BAY11-7082 [10 µM], on JMJD3 expression in MCD-treated BMDMs. (***C***) JMJD3 expression in cholesterol repletes MCD-treated macrophages. Graphs are representative of 3 independent experiments with 3 replicates per condition and are presented as means ± SD. Statistical analysis was performed using unpaired, two-tailed Student's t-test. An asterisk (*) or double asterisks (**) indicate a significant difference with $p<0.05$ and $p<0.001$, respectively. A hashtag (#) indicates a significant difference between MCD without or with inhibitors, $p < 0.05$.

Figure 2. Cellular cholesterol contents regulate NF-kB pathway. (***A***) TF regulatory pathways of activated genes were analyzed using Metascape; top TFs employed by either statin ***(a)*** or MCD ***(b)***; (***B***) NF-kB activation by MCD ***(a)*** and statins ***(b)*** using Raw blue^{TM} macrophages. RT-qPCR of IL-1β ***(c)*** and TNF-α ***(d)*** in RAW 264.7 cells with or without MCD (5 mM; 1 h), or with or without statins (7 µM + 200 µM mevalonate; 2 days). Effect of NF-kB inhibitors (MG-132 [5 µM] and BAY11-7082 [10 µM]) on IL-1β ***(e)*** and TNF-α ***(f)*** expression in MCD-treated RAW 264.7 macrophages. An asterisk (*) indicates a significant difference with $p<0.01$, respectively. A hashtag (#) indicates a significant difference between MCD without or with inhibitors with $p < 0.05$.

Figure 3. Cholesterol levels modulate mitochondrial respiration. (***A***) Mitochondrial oxygen consumption rates (OCR) of BMDMs treated with 1 h MCD (5 mM) or without. ***(a)*** OCR for mitochondrial resting respiration; ***(b)*** OCR representing mitochondrial ATP production-linked respiration. ***(c)*** OCR representing maximal respiration. (***B***) Mitochondrial oxygen consumption rates (OCR) in BMDMs treated statin or without. ***(a)*** OCR for mitochondrial resting respiration; ***(b)*** OCR representing mitochondrial ATP production-linked respiration; ***(c)*** OCR representing maximal respiration. Data are representative of 3 independent experiments with 3 samples per group and data are presented as mean ± SD. Statistical analysis was performed using unpaired, two-tailed Student's t-test. An asterisk (*) and (**) indicate a significant difference with with $p<0.05$ and $p<0.001$.

Figure 4. Cholesterol levels modulate the mitochondrial ATP synthase activity. (***A***) sterol 27-hydroxylase, CYP27A1, expression in 1 h MCD-treated and control RAW macrophages. (***B***) 27-hydroxycholesterol (27-HC) analysis by ultraperformance liquid chromatography/electrospray ionization/tandem mass spectrometry. 27-HC levels were normalized to the protein content in the whole cell pellet; (***C***) ATP hydrolysis and synthesis in cholesterol-doped inner membrane vesicles (IMVs); ATP hydrolysis was performed by adding a total concentration of 2 mM ATP to

200 mM IMVs (lipid concentration) and incubated for 30 minutes. Concentration of phosphates from ATP hydrolysis were measured using the malaquite green assay. ATP concentration after synthesis was measured using ATP detection assay kit (Molecular Probes) with a luminometer GloMax®-Multi Detection. Data in B are from 3 samples per group and data are presented as mean ± SD. An asterisk (*) indicates $p<0.05$. Data in (C) are representative of at least two independent experiments with three replicates and presented as means± SD. Statistical analysis was performed using the Tukey ANOVA test. (*), (**) and (***) indicate a significant difference with $p < 0.05$, 0.01 and 0.001, respectively.

Figure 5. Effect of proton flux on NF-kB activation and JMJD3 expression in MCD-treated cells. (***A***) Schematic of potential mechanism induced by MCD, and MCD/CCCP on mitochondrial proton flux. (***B***) Effect of CCCP on NF-kB activity and JMJD3 expression: ***(a)*** on NF-kB activity in Raw blue™ macrophages (CCCP = 50 µM); ***(b)*** on JMJD3 expression in RAW 264.7 macrophages (CCCP = 50 µM) and ***(c)*** BMDMs (CCCP = 200 µM). (***C***) Effect of CCCP on Il-1β expression in RAW 264.7 macrophages (CCCP = 50 µM). Data are representative of 3 independent experiments with 3 samples per group and data are presented as mean ± SD. Statistical analysis was performed using unpaired, two-tailed Student's t-test. Asterisk (*) and (**) indicate a significant difference with with $p<0.05$ and $p<0.001$. A hashtag (#) indicates a significant difference between MCD without or with inhibitors with $p < 0.05$.

Figure 6. Cholesterol modulates macrophage epigenetic modifications and LPS response. (***A***) Volcano plot of differentially accessible peaks between MCD-treated and control RAW 264.7 macrophages. (***B***) a RAW 264.7 macrophages treated with statin or without were stimulated with LPS (100 ng/ml) for 3 h. ***(a)*** Heatmap of LPS-activated genes that down regulated by statin; ***(b)*** GO analysis of LPS-activated genes that down-regulated by statin. ***(c)*** IL-10 upregulation in statin-treated macrophages. (***C***) The effect of JMJD3 demethylation in LPS stimulated RAW macrophages. ***(a)*** Expression of the JmjC demethylase family genes in macrophages with or without 1 h MCD treatment. ***(b)*** JMJD3 expression in MCD-treated macrophages. ***(c)*** the effect of MCD on raising IL-10/TNF-α ratio is dependent on the presence of glutamine. (***d***) effect of GSJK4, a JMJD3 inhibitor, on IL-10/TNF-α ratio. Data are representative of 3 independent experiments with 3 samples per group and data are presented as mean ± SD. Statistical analysis was performed using unpaired, two-tailed Student's t-test. An asterisk (*) and (**) indicate a significant difference with with $p<0.05$ and $p<0.001$. A hashtag (#) indicates a significant difference between MCD without or with glutamine with $p < 0.05$.

Figure 7: Statins suppress proinflammatory phenotypes and enhance the expression of anti-inflammatory factors, depending on glutamine, in BMDMs. (***A***) BMDMs treated with or without statins are stimulated by LPS (50 ng/ml, 3 h) and gene expressions are analyzed by qPCR. (***B***) BMDMs treated MCD were stimulated with LPS in the presence of glutamine or without. Expression of IL-10 and TNF-α were analyzed by qPCR to generate the ratio of ratio of IL-10/TNF-α. (***C***) BMDMs treated with or without statins are stimulated by IL-4 (20 ng/ml, 6 h) and gene expressions are analyzed by qPCR. (***D***) BMDMs treated with MCD were stimulated with IL-4 (20 ng/ml, 6 h) in the presence of glutamine or without. Expression of M2 genes were analyzed by qPCR. (***E***) Chromatin-immunoprecipitation (ChIP) analysis of H3K27me3 in BMDMs with or

without statin treatment. The inactive gene *desert* is used as input control. Data are representative of at least 2 independent experiments with 3 samples per group and data are presented as mean ± SD. Statistical analysis was performed using unpaired, two-tailed Student's t-test. An asterisk (*) and (**) indicate a significant difference with with $p<0.05$ and $p<0.001$. A hashtag (#) indicates not significant.

SUPPLEMENTARY FIGURES

Supplementary Figure 1. Western blot of H3K27Me3 site in macrophages treated with statins (2 d) or MCD (1h). Actin was used as a loading control and pCreb as indicator for effective cholesterol reduction.

Supplementary Figure 2. The gene expression activated by MCD, statin or LPS. RT-qPCR of IL-1β (**a**) and TNF-α (**b**) in RAW 264.7 cells with or without MCD (5 mM; 1 h), statins (7 µM + 200 µM mevalonate; 2 days) or LPS (100 ng/ml; 3 h). Graphs are representative of 3 independent experiments with 3 replicates per condition and are presented as means ± SD. Statistical analysis was performed using unpaired, two-tailed Student's t-test. An asterisk (*) or double asterisks (**) indicate a significant difference with $p<0.05$ and $p<0.001$, respectively.

Supplementary Figure 3. Cholesterol levels modulate mitochondrial respiration in RAW 264.7 macrophages. (***A***) Mitochondrial oxygen consumption rates (OCR) of RAW 264.7 macrophages in 5 mM MCD-treated or control macrophages. (**a**) OCR for mitochondrial resting respiration; **b**) OCR representing mitochondrial ATP production-linked respiration. (**c**) OCR representing maximal respiration. **(B)** Mitochondrial oxygen consumption rates (OCR) in statin-treated or control RAW 264.7 macrophages (**a**) OCR for mitochondrial resting respiration; **b**) OCR representing mitochondrial ATP production-linked respiration. (**c**) OCR representing maximal respiration. **(C)** Effect of proton flux on NF-kB activation in MCD-treated cells. Data are representative of three independent experiments and presented as means± SD. Statistical analysis was performed using unpaired, two-tailed Student's t-test. An asterisk (*) or double asterisks (**) indicate a significant difference with $p<0.05$ and $p<0.001$, respectively.

Supplementary Figure 4. Sterol 27-hydroxylase, CYP27A1, expression. RAW 264.7 macrophages were treated with statin for 2 d and the expression of CYP27A1 analyzed. $P<0.01$.

Supplementary Figure 5. Inhibitor of proton flux in mitochondria on NF-kB pathway. Effect of BAM15 (200 µM) on Il-1β ***(a)*** and JMJD3 ***(b)*** gene expression in MCD-treated RAW264.7 cells. Data are representative of 3 independent samples per condition and are presented as mean ± SD. Statistical analysis was performed using unpaired, two-tailed Student's t-test. asterisk (*) and hashtag (#) indicate a significant difference between MCD without or with inhibitors with $p < 0.05$.

Supplementary Figure 6. RAW macrophages treated with MCD or without were stimulated with LPS (100 ng/ml) for 3 h. ***(a)*** Heatmap of LPS-stimulated genes that down regulated by statin; ***(b)*** GO analysis of LPS-stimulated genes that down-regulated by statin.

Supplementary Figure 7. Expression of the JmjC demethylase family genes in 264.7 macrophages with or without statin treatment (2 days). An asterisk (*) indicates a significant difference with with $p<0.001$.

Materials and Methods

Reagents and chemicals

Cell culture Dulbecco's Modified Eagle Medium (DMEM) was purchased from Gibco (Thermo Fisher Scientific, Watham, MA). Antibiotics (penicillin and streptomycin) and fatty acid (FA)-free bovine serum albumin (BSA) were purchased from Sigma-Aldrich (St Louis, MO). FBS (Optima) was purchased from Atlanta Biologicals (R&D systems; Minneapolis, MN). As for the chemicals, the following inhibitors: MG-132 (proteasome inhibitor), BAY11-7082 (IKK inhibitor), and BAM15 (another mitochondrial uncoupler) were purchased from TOCRIS chemicals (part of R&D systems). Methyl-β-cyclodextrin (MCD), simvastatin, mevalonate, oligomycin, rotenone, antimycin A, carbonyl cyanide 3-chlorophenylhydrazone (CCCP), 4-(2-hydroxyethyl)- 1-piperazineethanesulfonic acid (HEPES), and phosphate-buffered saline (PBS) were purchased from Sigma-Aldrich. For the IMVs study, magnesium chloride ($MgCl_2$), 2-(N-morpholino) ethanesulfonic (MES), sucrose, hexane, bovine serum albumin (BSA), sulfuric acid (H_2SO_4), hydrochloric acid 37% (HCl), sodium chloride (NaCl), potassium chloride (KCl), dibasic potassium phosphate (K_2HPO_4), sodium hydroxide (NaOH), Hydrogen peroxide (H_2O_2), trichloroacetic acid (TCA), adenosine 5'-triphosphate disodium salt hydrate (Na_2ATP), adenosine 5'-diphosphate sodium salt (Na_2ADP), and cholesterol were also supplied by Sigma-Aldrich. Ammonium molybdate (VI) tetrahydrate and L-ascorbic acid were purchased from Acros Organics (part of Sigma Aldrich). Ultrapure water was produced from a Milli-Q unit (Millipore, conductivity lower than 18 MΩ cm). Rabbit anti-mouse JMJD3 primary antibody was lab-generated as described in[1]. The following antibodies were acquired from several vendors: mouse monoclonal anti-β-actin antibody (A1978) from Sigma-Aldrich, rabbit anti-mouse pCREB (87G3), rabbit anti-mouse CREB (86B10), and rabbit anti-mouse Tri-Methyl-Histone H3 (Lys27) antibodies were from Cell Signaling technology (Danvers, MA). The secondary antibody HRP-conjugated anti-rabbit antibody was from Cayman chemicals (Ann Arbor, MI). The Enhanced chemiluminescence (ECL) solutions for the Western blotting system were from GE Healthcare (Chicago, IL). The protease and phosphatase inhibitor cocktails were purchased from Sigma-Aldrich.

RAW264.7

The RAW 264.7 murine macrophage cell line (American Type Collection Culture [ATCC]; Manasas, VA) was maintained in 100-mm diameter tissue culture-treated polystyrene dishes (Fisher Scientific, Hampton, NH) at 37°C in a humidified atmosphere of 95% air and 5% CO_2. The cells were cultured in DMEM-based growth medium containing glutamine and without pyruvate, supplemented with 10% [v/v] heat-inactivated fetal bovine serum (FBS) and 1x Penicillin/ streptomycin). For experiments (and routine subculture), cells were collected in growth media after 25 minutes incubation with Accutase (Sigma Aldrich, St Louis, MO) at 37°C in a humidified atmosphere of 95% air and 5% CO_2. In preparation for experiments, cells were seeded in 6-well tissue culture-treated polystyrene plates (Fisher Scientific, Hampton, NH) at 30,000 cells/cm^2 for 2 days until cells have recovered in time for treatments. Unless otherwise indicated, cell treatments were prepared in DMEM supplemented with 0.25% (w/v) FA-free BSA that was sterilized by filtration through 0.2-µm pore size cellulose acetate syringe filters. For treatments, cells were washed with pre-warmed sterile PBS and were treated with media containing MCD (5

mM), cell culture-grade water (negative control). Then, the cells were incubated for 1 hour under cell culture conditions. RAW 264.7 macrophages were pre-incubated for 5 minutes with CCCP (50 µM), 30 minutes with BAM15 (200 µM), or 1 hour with NF-kB inhibitors (MG-132 [5 µM] or BAY11-7082 [10 µM]).

Bone marrow-derived macrophages (BMDMs)

Bone marrow-derived macrophages (BMDM) were differentiated from bone marrow cells isolated from the femora, and tibiae of 4- to 16-week-old wild type C57BL/6J mice. Euthanasia was performed by CO_2 gas asphyxiation followed by cervical dislocation. Euthanized mice were soaked with 70% (v/v) ethanol immediately prior to dissection. After careful isolation of the bones, the ends of the bones were cut with sterile scissors and centrifuged at 10,000 rpm for 15 seconds at room temperature in a microcentrifuge (MCT) tube where the bone marrow is collected.
The bone marrow is then filtered using sterile, combined and centrifuged at 480 *g* for 10 minutes at room temperature. The cell pellet is resuspended briefly (< 2 minutes) in red blood cell lysis buffer. The differentiation medium (DMEM + 20% L-929-conditioned media + 10% FBS + 1% penicillin-streptomycin) is then added and cells are centrifuged again at 480 *g* for 10 minutes at room temperature. The cell suspension is filtered once more through a 70-µm strainer (into another 50 ml centrifuge tube to rinse and collect all the cells. 100-mm diameter suspension dishes (Greiner Bio-One, Monroe, NC) are seeded with 10 mL per dish at 0.6-0.8 x 10^6 cells/mL (~10,000-15,000 cells/cm^2). The dishes were then incubated for 6 days at 37°C in a humidified atmosphere of 95% air and 5% CO_2. Differentiation media (10 mL) are added on Day 3 or 4.
At the end of day 7, cells are detached with trypsin, counted and reseeded into 6-well plates at 0.5 million cells/well (~ 50,000 cells/cm^2) using 2mL/well of DMEM supplemented with 10% FBS and 1% P/S. Plates are left overnight at 37°C in a humidified atmosphere of 95% air and 5% CO_2 to ensure cell adherence. BMDMs are now ready to be used for assays.

RNA purification and cDNA synthesis

After treatment, the cells were lysed and collected in TRIzol (ThermoFisher Scientific, Watham, MA), and frozen at -80°C. Total RNA was extracted by phenol–chloroform extraction, followed by ethanol precipitation. RNA was purified through columns supplied in the Molecular Biology kit (BioBasic Inc., Markham, ON), according to the manufacturer's instructions. The RNA concentrations and purity were determined using a NanoDrop One (ThermoFisher Scientific, Watham, MA) spectrophotometer. cDNA synthesis was performed on the Bio-Rad T100 PCR Gradient Thermal Cycler using the QuantiTect® Reverse Transcription kit (Qiagen, Germantown, MD), following manufacturer´s instructions.

Reverse transcriptase quantitative PCR (RT-qPCR)

Gene expression was analyzed by real time reverse transcriptase quantitative PCR (RT-qPCR) according to the Fast SYBR Green protocol with the AriaMx real-time PCR detection system (Agilent technologies, Santa Clara, CA). Primers were ordered from Invitrogen (ThermoFisher Scientific, Watham, MA) and are listed in Table 1. Each condition was prepared in triplicates and

each sample was loaded as technical triplicates for each gene (target or reference) analyzed. The mRNA levels of mouse HPRT1 or GAPDH were used as internal controls (reference gene) as indicated.

Table 1: Mouse primers used for real time RT-qPCR

Primer	**Sequence**	
HPRT1	Forward	TGTTGTTGGATATGCCCTTG
	Reverse	TTGCGCTCATCTTAGGCTTT
IL-1β	Forward	AGTTGACGGACCCCAAAAGAT
	Reverse	GTTGATGTGCTGCTGGGAGA
JMJD3	Forward	CCAGGCCACCAAGAGAATAA
	Reverse	CGCTGATGGTCTCCCAATAG
TNF-α	Forward	CCGTAGGGCGATTACAGTCA
	Reverse	CCTGGCCTCTCTACCTTGTTG
IL-10	Forward	TGGCCCAGAAATCAAGGAGC
	Reverse	CAGCAGACTCAATACACACT
IL-6	Forward	TAGTCCTTCCTACCCCAATTTCC
	Reverse	TTGGTCCTTAGCCACTCCTTC
IL-12b	Forward	GGAAGCACGGCAGCAGAATA
	Reverse	AACTTGAGGGAGAAGTAGGAATGG
Arg1	Forward	CTCCAAGCCAAAGTCCTTAGAG
	Reverse	AGGAGCTGTCATTAGGGACATC
Ym1	Forward	AGAAGGGAGTTTCAAACCTGGT
	Reverse	GTCTTGCTCATGTGTGTAAGTGA
Mrc1	Forward	CTCTGTTCAGCTATTGGACGC
	Reverse	CGGAATTTCTGGGATTCAGCTTC

Immunoblotting

For Western blot analysis, MCD-treated RAW 264.7 cells were washed in ice-cold PBS, lysed in radioimmune precipitation assay (RIPA) buffer (150 mM NaCl, 1% Nonidet P-40, 1% sodium deoxycholate, and 25 mM Tris (pH 7.6)) supplemented with a cocktail of protease and phosphatase inhibitors. Total cell lysis was achieved through sonication for 20 seconds at 20% amplitude and samples were stored at -80°C. Histone extraction was performed following a specific protocol from Abcam. Protein concentration was determined using the Bradford assay (Bio-Rad, 5000006). SDS buffer (313 mM Tris (pH 6.8), 10% SDS, 0.05% bromophenol blue, 50% glycerol, and 0.1 M DTT) was added, and the samples were boiled at 100 °C for 5 minutes. Proteins were separated by SDS-PAGE on 10% acrylamide gels. After separation, proteins were transferred onto PVDF membranes and were blocked in 5% milk powder (in PBS, 1% Triton X-100) for 1 h. Membranes were incubated with the primary antibodies in the following conditions: overnight incubation with the anti-JMJD3 antibody (1:400) at 4°C, and 1h with the anti-H3K27Me3 antibody at room temperature. After washes, blots were further incubated with an HRP-conjugated anti-rabbit antibody (1:10 000) for 1h. Blots were imaged using ECL-based film detection system.

MCD/cholesterol (10:1 mol/mol) preparation

Cholesterol (0.3 mmol) of is dissolved in 1 ml chloroform solution and dried under nitrogen in a glass culture tube. 10 ml of a MCD solution (300 mM) prepared in BSA/BSS buffer solution (20 mM Hepes, pH 7.4, 135 mM NaCl, 5 mM KCl, 1.8 mM $CaCl_2$, 1 mM $MgCl_2$, 5.6 mM glucose, and 1 mg/ml BSA) was added to the tube, and the resulting suspension was vortexed, and bath-sonicated at 37°C until the suspension clarified. The suspension was then incubated in a rocking water bath overnight at 37°C to maximize formation of soluble complexes. This is the stock solution that can be diluted into desired concentrations.

Macrophage cholesterol depletion and repletion.

On the day of experiment, RAW264.7 cells are incubated with 5 mM MCD for 1 h. The cells are rinsed in 0.25% BSA in DMEM and left to rest for 10 minutes before switching the media to media containing MCD/cholesterol complex at these specific concentrations: 10, 5, 3, 1 mM MCD/cholesterol complex, for 1 h. RNAs are collected at the end of incubation for JMJD3 expression. Controls cells will be cells that did receive any treatment or MCD. Triplicates wells are prepared for the concentration of control, MCD, and the optimal MCD + MCD/cholesterol complex concentration where JMJD3 expression could be properly rescued, i.e. JMJD3 goes back the closest to baseline level.

NF-kB activation assay

NF-kB activation was determined by performing the QUANTI-Blue assay using the RAW-Blue™ cells (InvivoGen). Through exposure of the RAW-Blue cells to various substances, NF-kB/AP-1 activation is induced, making secreted embryonic alkaline phosphatase (SEAP) into the cell supernatant. In brief, RAW-Blue cells were seeded in 6-well plates (1.5×10^5 cells/ml), and were allowed to recover for 2 days in growth media (similar to RAW264.7 cells) before they were stimulated with LPS (100 ng/ml) or MCD (5 mM) for 3h. Then, the cells and medium for each sample were collected and sonicated on ice for 15 seconds at 20% amplitude. The supernatant was separated from cell debris by centrifugation at 4°C for 10 minutes at 10,000 rpm. For detection, the cell supernatant and a secreted embryonic alkaline phosphatase (SEAP) detection reagent (QUANTI-Blue) were mixed and the absorbance was measured at 650 nm as described in the assay instructions. Each condition was performed in triplicate samples and each sample was measured in technical triplicates.

Mitochondrial Oxygen Consumption

Cellular oxygen consumption rates (OCR) were measured using an extracellular flux analyzer (Seahorse XF96e; Agilent Technologies, Santa Clara, CA). Briefly, the cartridge sensors were incubated overnight at 37 °C in a hydration/ calibration solution (XF Calibrant; Agilent Technologies). Specially designed polystyrene tissue culture-treated 96-well microplates with a clear flat bottom (Seahorse XF96 V3 PS Cell Culture Microplates; Agilent Technologies) were then seeded with 80 µl of cell suspension (4.4×10^5 cells/ml) per well and incubated 2–3 h under cell

culture conditions to allow cell attachment. For treatment with MCD, cells were washed with pre-warmed sterile PBS and the culture supernatants were replaced with medium containing MCD (5 mM). Then, the cells were incubated for 1 h under cell culture conditions. For treatment with statins, cells were washed with pre-warmed sterile PBS and the culture supernatants were replaced with medium supplemented with lipoprotein-deficient serum (LPDS), containing statins (7 μM lovastatin + 200 μM mevalonate). Then, the cells were incubated for 2 days under cell culture conditions. At the end of either treatment, the cells are washed and incubated 45 minutes at 37 °C in extracellular flux analysis medium (sodium bicarbonate-, glucose-, phenol red-, pyruvate-, and glutamine-free modified DMEM [Sigma-Aldrich, catalog no. D5030] freshly supplemented with cell culture-grade D-glucose (4.5 g/L), cell culture-grade L-glutamine [4 mM; Wisent], and 4-(2-hydroxyethyl)-1-piperazineethanesulfonic acid [HEPES; 4.5 mM; Sigma-Aldrich], pH adjusted to 7.35-7.40 at room temperature). OCR were measured to assess resting respiration, followed by ATP production-dependent respiration, maximal respiration, and non-mitochondrial oxygen consumption, after sequential injections of oligomycin (an ATP synthase inhibitor) at 1μM (final concentration), CCCP (an ionophore acting as a proton uncoupler) at 2μM, and rotenone together with antimycin A (complex I and complex III inhibitors, respectively), each at 0.5μM. mitochondrial ATP production-dependent respiration was calculated by subtracting the lowest OCR after oligomycin injection from resting OCR. For each parameter, OCR measurements were performed at least three times at 6-minute intervals. Each condition was performed in 7–8 replicates samples. All OCR measurements were corrected for the OCR of cell-free wells containing only medium. Upon completion of the OCR measurements, the cells were washed once with PBS and lysed in 1M NaOH (40 µl/well). The lysates were kept at 4 °C for up to 24 h, and protein determination was performed using the Bradford colorimetric assay with BSA as the standard protein (Thermo Scientific). Absorbance was measured at a wavelength of 595nm using a hybrid microplate reader (Biotek).

27-Hydroxycholesterol (27-HC) quantification

Cell pellets were collected from RAW264.7 macrophages treated with 1, 3 and 5 mM of MCD for 1 hour. Samples were sent to the University of Texas (UT) Southwestern Medical center for analysis by ultraperformance liquid chromatography/electrospray ionization/tandem mass spectrometry allowing chromatographic resolution of the hydroxycholesterol species. 27-HC levels were calculated by normalizing the 27-HC amounts to the protein content in the whole cell pellet.

Purification and formation of E. coli inner membrane vesicles (IMVs)

E. coli inner membranes were purified from *E. coli* MG1655 strain by sucrose gradient ultracentrifugation (30 minutes at 80,000 rpm, Optima™ MAX-XP) as previously described[2]. The *E.coli* inner membranes were then resuspended in either the synthesis buffer (MES 100 mM pH 6 and NaCl 25 mM) or the hydrolysis buffer (HEPES 25 mM pH 8) and ultrasonicated for 15 minutes (5 seconds on-off cycles at 30% power, VCX500 Ultrasonic Processors). The resulting homogeneous solution contained the inner membrane vesicles (IMVs).

Loading and depletion of cholesterol in IMVs

Prior to any treatment, the protein concentration of IMVs was determined by the BCA protein assay and IMVs were diluted to a final protein concentration of 0.5 mg/ml. IMVs were then loaded with cholesterol using a modified protocol based on the MCD/cholesterol complex[3]. To load IMVs, 25 mM MCD were mixed with 2.5 mg/ml of cholesterol on HEPES (25 mM, pH7.8) following the protocol described in[4]. After incubation with MCD-cholesterol complexes, IMVs were ultracentrifuged (80,000 rpm for 30 minutes) and the supernatant removed. The IMVs were then resuspended in HEPES 25 mM (pH 7.8). After loading, the lipid, cholesterol and protein concentration of IMVs were determined by the phosphate determination assay[5], Amplex Red cholesterol assay kit[6] and BCA protein assay[7], respectively. To achieve vesicles with different cholesterol content, cholesterol-loaded IMVs (1mg/mL protein concentration) were treated with increasing MCD concentrations (from 0 to 7.0 mM) for 30 minutes at 37°C[3, 8]. Cholesterol-depleted vesicles were ultracentrifuged (80000 rpm for 30 minutes) and the pellet was resuspended in HEPES (25 mM, pH=7.8). Lipid, protein and cholesterol concentration of depleted samples were quantified again after the MCD treatment.

Hydrolysis and synthesis of ATP on cholesterol-doped IMVs

ATP hydrolysis was performed by adding a total concentration of 2 mM ATP to 200 mM IMVs (lipid concentration) and incubated for 30 minutes. The concentration of phosphates from ATP hydrolysis was measured using the malaquite green assay[9]. ATP synthesis was triggered by promoting a ΔpH across the IMV membranes by mixing the samples (IMVs resuspended in MES 100 mM pH 6) with an external buffer with higher pH and in the presence of inorganic phosphate, ADP and magnesium ion (HEPES 100 mM pH 8, 5 mM P_i, 2.5 mM ADP, 5 mM $MgCl_2$, 25 mM NaCl) at a volume ratio of 1:10 and incubated for 2 to 5 minutes. The reaction was stopped by adding 20% TCA at a ratio volume of 10:1, and then the samples was equilibrated to neutral pH[10]. ATP concentration after synthesis was measured using ATP detection assay kit (Molecular Probes) with a luminometer GloMax®-Multi Detection. Amplex™ Red Cholesterol Assay Kit and Pierce® BCA Protein assay kits were supplied by ThermoFisher. Luminescent ATP Detection Assay Kit (based on firefly's luciferase / luciferin) was purchased from Molecular Probes.

RNA-sequencing

RAW 264.7 macrophages in duplicates were either left untreated or treated with 5 mM MCD for 1 hour. Total RNA was purified as described above, and the RNA concentrations and purity were determined using a NanoDrop One (ThermoFisher Scientific, Watham, MA) spectrophotometer. Library preparation and 150-bp paired-end RNA-Seq were performed using standard Illumina procedures for the NextSeq 500 platform. The RNA-Seq data were analyzed using the Bowtie, TopHat, CuffLinks, and CummeRbund software suite[11]. Briefly, reads were mapped to the mm9 genome (University of California, Santa Cruz, California, USA) and known mm10 transcripts (RefSeq mm10 build37.2) using Bowtie version 2.2.4[12] with default parameters. Splice junctions were determined from the mapped reads using TopHat version 2.0.12[13] with default values. Transcript quantification was performed with HT-Seq version 0.6.1[14]. Identification of differentially expressed genes was performed with the edgeR Bioconductor package[15]. RNA-Seq data were deposited in the UCSC genome browser database.

ATAC-seq

RAW 264.7 macrophages in duplicates were either left untreated or treated with 5 mM MCD for 1 hour. Cells were detached using 0.5% trypsin and resuspended in chilled 1X PBS containing 1 mM EDTA. Visible cell numbers per sample were obtained by staining the cells with trypan blue and counting them using hemocytometer. 50,000 cells were used for performing ATAC-Seq. Cells were washed in 100 µl of ice cold 1X PBS and centrifuged at 500 x g for 5 minutes. Nuclei are prepared by lysing the cells in ice cold lysis buffer containing 10 mM Tris-Cl, pH7.4, 10 mM NaCl, 3 mM $MgCl_2$ and 0.1% IGEPAL CA-630. Nuclei were pelleted by spinning the samples at 500 x g for 10 minutes in fixed-angle cold centrifuge and proceeded for tagmentation reaction. A 25 µl tagmentation reaction was setup by resuspending the nuclei in 12.5 µl of 2x Tagment DNA buffer and 5 µl of TDE1 transposase. Samples were incubated at 37°C for 30 minutes with gentle intermittent mixing. Following transposition, the sample volume was made up to 50 µl using resuspension buffer and were processed for DNA preparation. For tagmented DNA clean-up, 180 µl of Zymo DNA binding buffer was added and mixed thoroughly before loading on to Zymo-spin concentrator-5 columns. For transposase free DNA, the samples were eluted in 16.5 µl of elution buffer. Purified tagmented DNA was amplified with KAPA HIFI polymerase (12 PCR cycles) and Unique Dual Primers from Illumina (Cat number 20332088). Size-selection (L:1.1; R :0.6) was performed with KAPA Pure beads and size distribution of the final libraries was assessed on bioanalyzer (Agilent). Libraries were quantified by qPCR and loaded equimolarly on a S4 Novaseq flowcell. Each library was sequenced with a coverage of 50M paired-end reads (PE100).

ATAC-seq analysis

FastQC[16] was used to perform preliminary quality-control for paired-end FASTQ reads retrieved for control and MCD-treated samples (two replicates each) respectively. Sequencing adapters were trimmed from the reads using Cutadapt v2.6[17] and aligned to the mouse genome (GRCm38-mm10) using Bowtie2 v2.4.4[12]. The resulting alignments were filtered using Samtools v1.10[18] to retain those that were mapped in proper pairs (-f 2) and based on their MAPQ scores (-q 10). Finally, duplicates were removed using Picard (java v1.8.0) and the resulting filtered alignments were converted to genome-browser compatible 24igwig files with CPM normalization using bamCoverage (deeptools v3.5.1)[19]. The filtered alignments were concurrently also used to identify (narrow) peaks for each of the replicates using MACS3 v3.0.0[20] with default parameters. Differential peaks between control and MCD-treated samples were identified using DiffBind[21] and functional annotation of peaks was performed using ChIPseeker[22].

Statistical analysis

Statistical analyses between data groups were performed with PRISM software (GraphPad). Data for real time RT-qPCR and Seahorse experiments are presented as the mean ± S.D. as indicated. The statistical significance of differences between groups was analyzed by Student's *t* test. Differences were considered significant at a p value < 0.05.

References

1. Benyoucef A. *et al.* UTX inhibition as selective epigenetic therapy against TAL1-driven T-cell acute lymphoblastic leukemia. *Genes Dev.* **30**, 508-521 (2016).

2. Gutiérrez-Sanz O. *et al.* H2-Fueled ATP Synthesis on an Electrode: Mimicking Cellular Respiration. *Angewandte Chemie*, 6216– 6220 (2016).

3. Mahammad S. & Parmryd I. Cholesterol depletion using methyl-β-cyclodextrin, in *Methods in Membrane Lipids. Methods in Molecular Biology*, Vol. 1232. (ed. I.O. D.) (Humana Press, New York, NY; 2015).

4. Bacia K., Scherfeld D., Kahya N. & Schwille P. Fluorescence correlation spectroscopy relates rafts in model and native membranes. *Biophysical Journal* **87**, 1034-1043 (2004).

5. Chen P.S., Toribara J.T.Y. & H., W. Microdetermination of phosphorus. *Analytical Chemistry*, 1756-1758 (1956).

6. Amundson D.M. & Zhou M. Fluorometric method for the enzymatic determination of cholesterol. *Journal of Biochemical and Biophysical Methods* **38**, 43-52 (1999).

7. Smith P.K. *et al.* Measurement of protein using bicinchoninic acid. *Analytical Biochemistry* **150**, 76-85 (1985).

8. Pucadyil T.J. & Chattopadhyay A Cholesterol depletion induces dynamic confinement of the G-protein coupled serotonin1A receptor in the plasma membrane of living cells. *Biochimica et Biophysica Acta (BBA) - Biomembranes* **1768**, 655-668 (2007).

9. Lanzetta P. A., Alvarez L. L. J., Reinach P S. & A., C.O. An improved assay for nanomole amounts of inorganic phosphate. *Analytical Biochemistry* **100**, 95-97 (1979).

10. Kaim G. & Dimroth P. Construction, expression and characterization of a plasmid-encoded Na(+)-specific ATPase hybrid consisting of Propionigenium modestum FO-ATPase and Escherichia coli F1-ATPase. *Eur J Biochem*, 615-623 (1994).

11. Trapnell C. *et al.* Differential gene and transcript expression analysis of RNA-seq experiments with TopHat and Cufflinks. *Nat Protoc.* **7**, 562–578 (2012).

12. Langmead B. & Salzberg S. Fast gapped-read alignment with Bowtie 2. *Nature Methods* **9**, 357-359 (2012).

13. Trapnell C., Pachter L. & Salzberg S.L. TopHat: discovering splice junctions with RNA-Seq. *Bioinformatics* **25**, 1105-1111 (2009).

14. Anders S., Pyl P.T. & Huber W. HTSeq—a Python framework to work with high-throughput sequencing data. *Bioinformatics* **31**, 166-169 (2015).

15. Robinson M.D., McCarthy D.J. & Smyth G.K. edgeR: a Bioconductor package for differential expression analysis of digital gene expression data. *Bioinformatics* **26**, 139-140 (2010).

16. Andrews S. FastQC: A quality control tool for high throughput sequence data *[Online]* (2010).

17. Martin M. Cutadapt removes adapter sequences from high-throughput sequencing reads. *EMBnet.journal* **17**, 10-12 (2011).

18. Li H. *et al.* The sequence alignment/map format and samtools. *Bioinformatics* **25**, 2078-2079 (2009).

19. Ramirez F. *et al.* deepTools2: a next generation web server for deep-sequencing data analysis. *Nucleic Acids Res.* **44**, W160-165 (2016).

20. Zhang Y. *et al.* Model-based Analysis of ChIP-Seq (MACS). *Genome Biol.* **9**, R137 (2008).

21. Ross-Innes C. S., S.R., Teschendorff A. E., Holmes K. A., Ali H. R., Dunning M. J., Brown G. D., Gojis O., Ellis I. O., Green A. R., Ali S., Chin S.F., Palmieri C., Caldas C., Carroll J. S. Differential oestrogen receptor binding is associated with clinical outcome in breast cancer. *Nature* **481**, 389-393 (2012).

22. Yu G., Wang LG. & He Q-Y. ChIPseeker: An R/Bioconductor Package for Chip Peak Annotation, Comparison and Visualization. *Bioinformatics* **31** 2382–2383 (2015).

Figure 1.

A

a

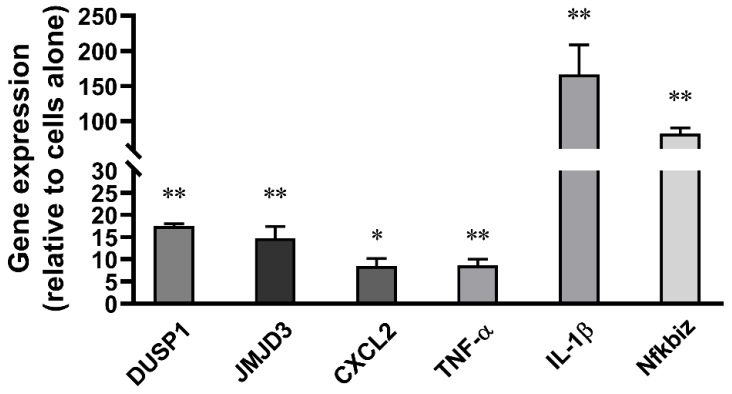

b

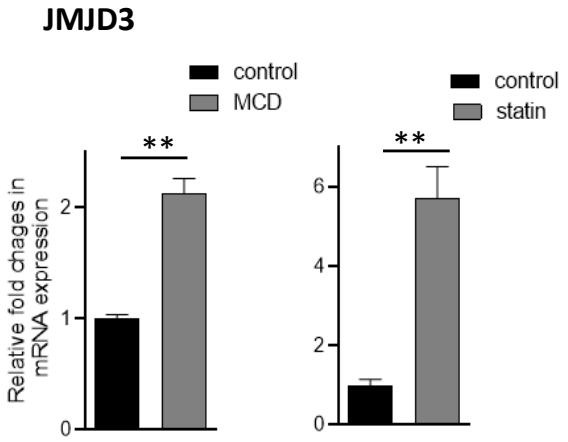

c

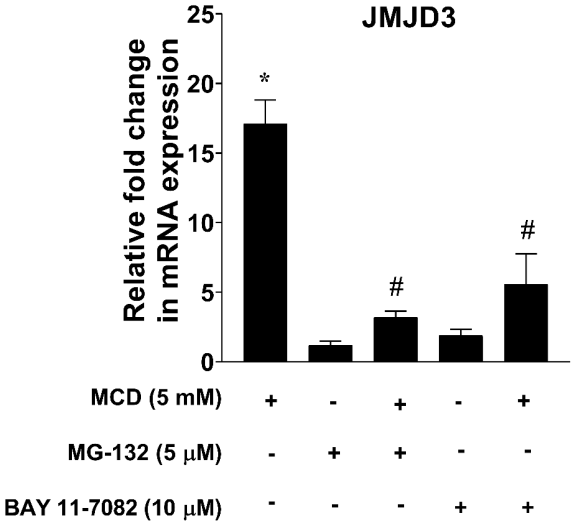

d

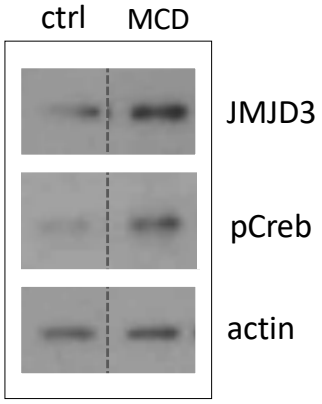

e

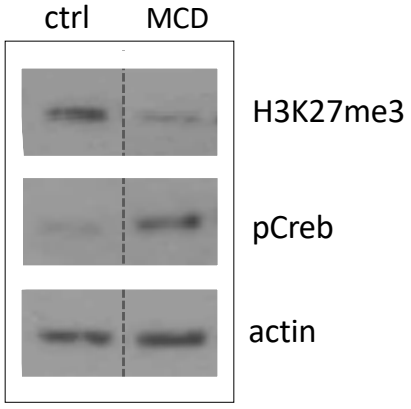

Figure 1.

B

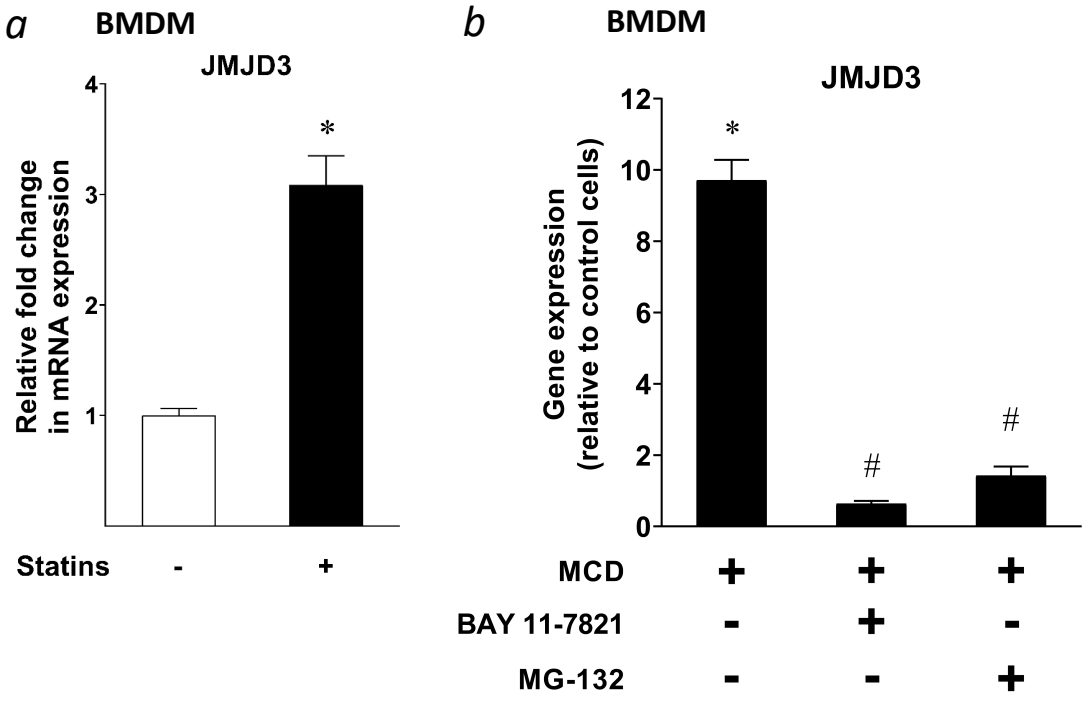
a
BMDM
JMJD3
Relative fold change in mRNA expression
4
3
2
1
*
Statins
-
+
b
BMDM
JMJD3
Gene expression (relative to control cells)
12
10
8
6
4
2
0
*
#
#
MCD
+
+
+
BAY 11-7821
-
+
-
MG-132
-
-
+

C

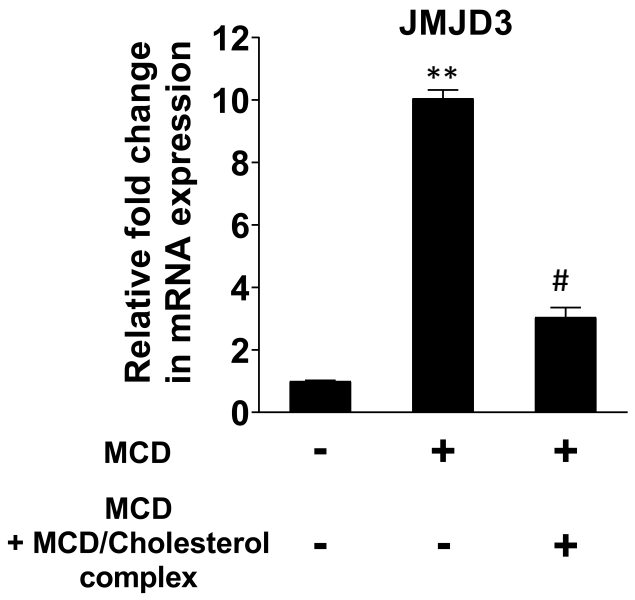
JMJD3
Relative fold change in mRNA expression
12
10
8
6
4
2
0
**
#
MCD
-
+
+
MCD
+ MCD/Cholesterol complex
-
-
+

Figure 2.

A

a

Statin

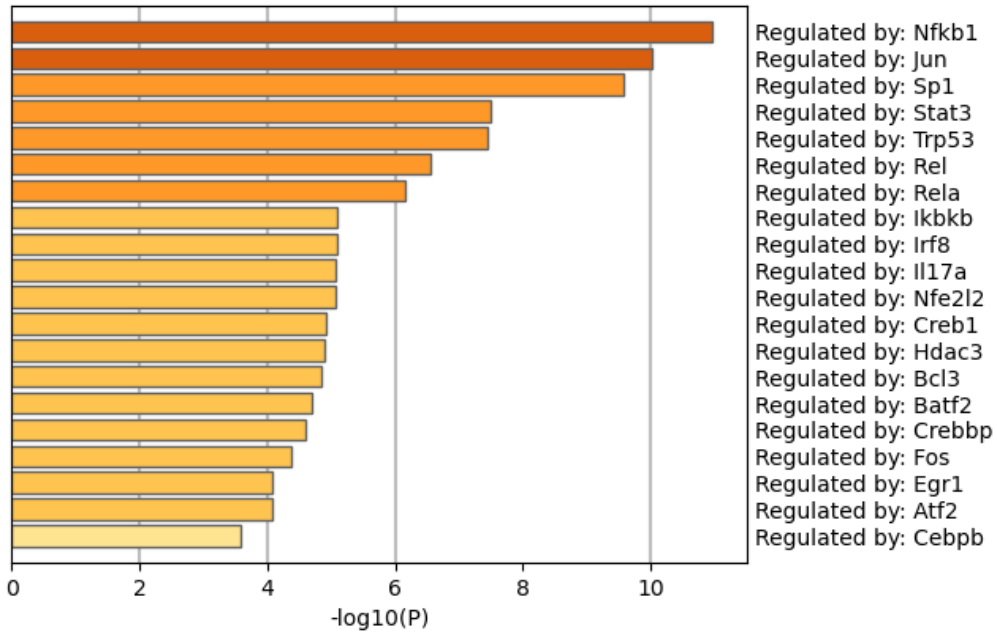

b

MCD

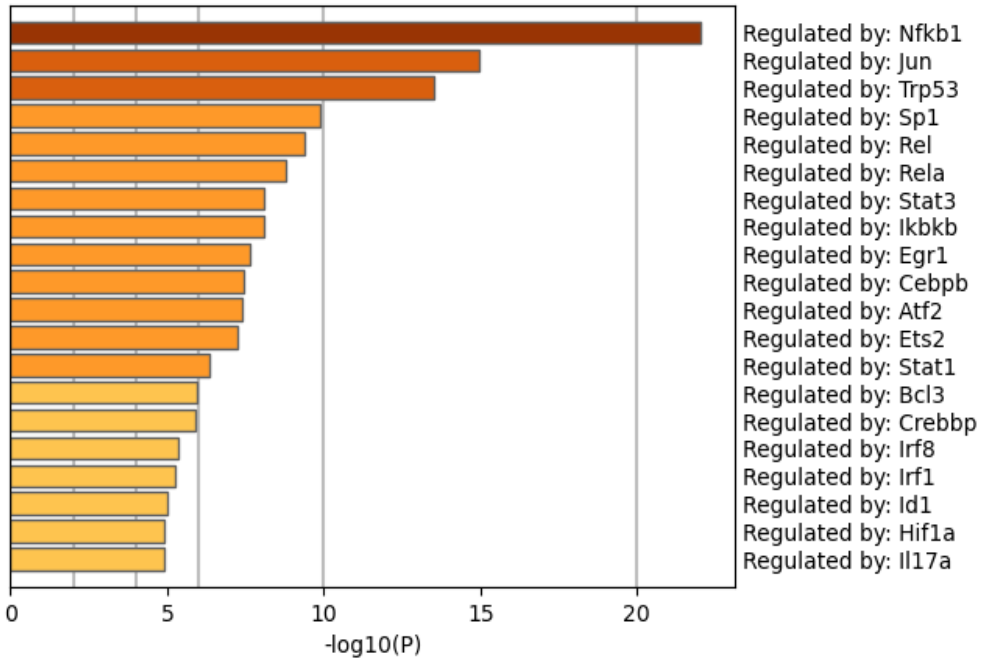

Figure 2.

B

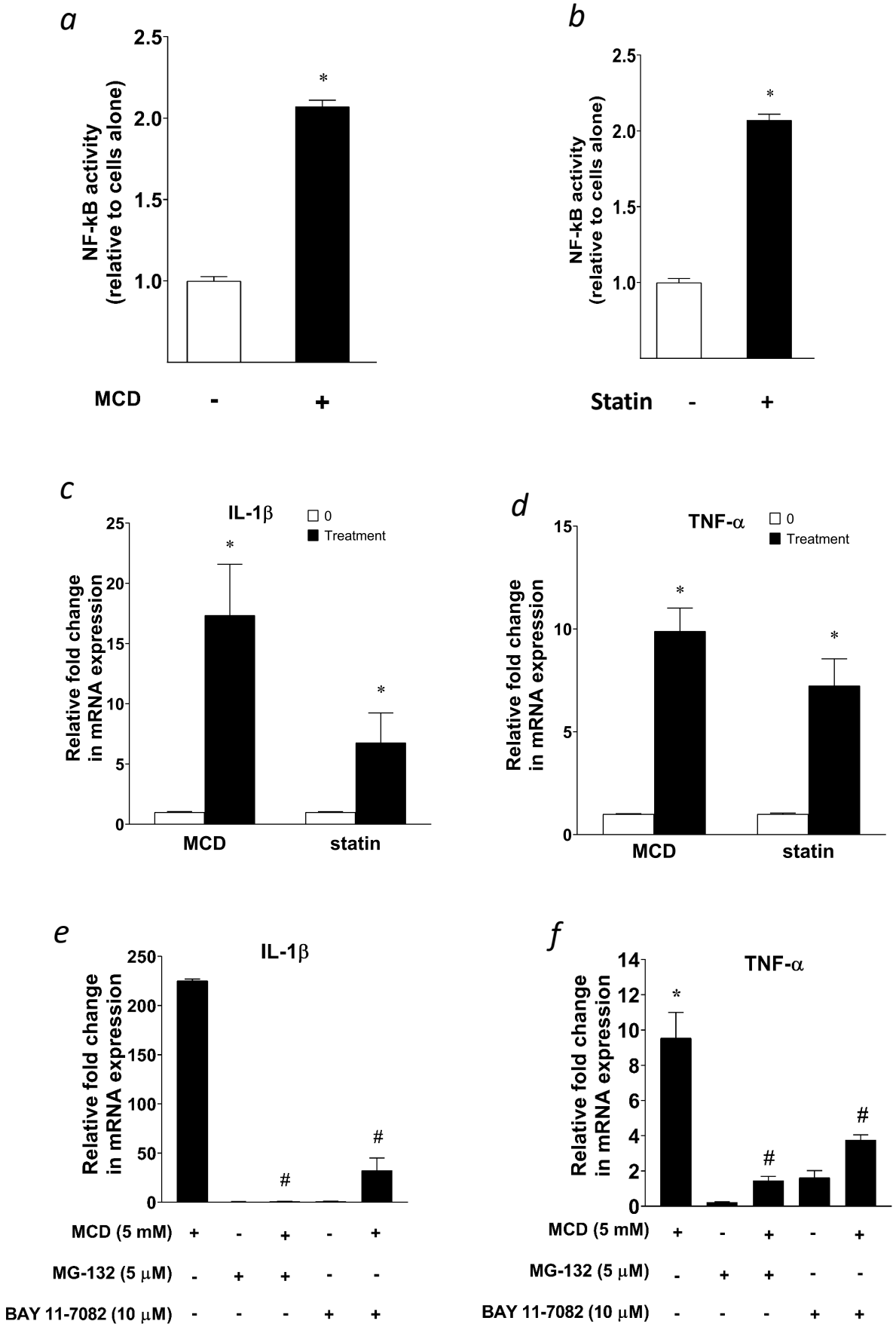
a
NF-kB activity
(relative to cells alone)
2.5
2.0
1.5
1.0
*
MCD
-
+
b
NF-kB activity
(relative to cells alone)
2.5
2.0
1.5
1.0
*
Statin
-
+
c
IL-1β
0
Treatment
Relative fold change
in mRNA expression
25
20
15
10
5
0
*
*
MCD
statin
d
TNF-α
0
Treatment
Relative fold change
in mRNA expression
15
10
5
0
*
*
MCD
statin
e
IL-1β
Relative fold change
in mRNA expression
250
200
150
100
50
0
#
#
MCD (5 mM) + - + - +
MG-132 (5 μM) - + + - -
BAY 11-7082 (10 μM) - - - + +
f
TNF-α
Relative fold change
in mRNA expression
14
12
10
8
6
4
2
0
*
#
#
MCD (5 mM) + - + - +
MG-132 (5 μM) - + + - -
BAY 11-7082 (10 μM) - - - + +

Figure 3.

A

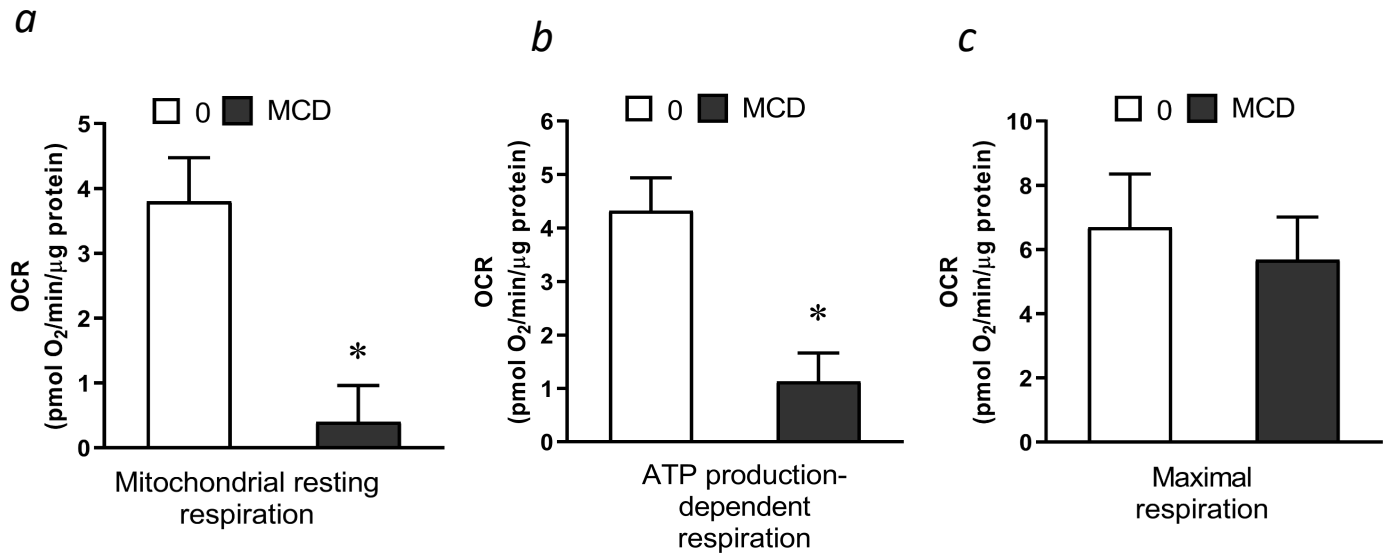
a
b
c
0
MCD
OCR
(pmol O2/min/µg protein)
*
Mitochondrial resting respiration
ATP production-dependent respiration
Maximal respiration

B

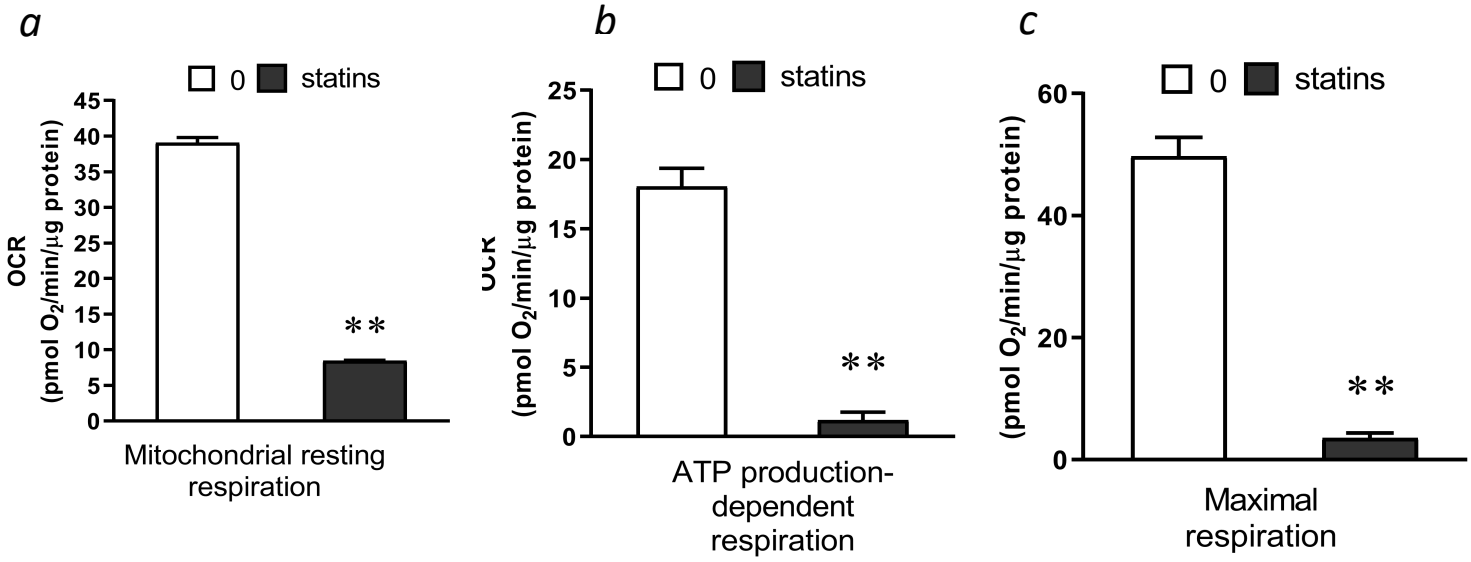
a
b
c
0
statins
OCR
(pmol O2/min/µg protein)
**
Mitochondrial resting respiration
ATP production-dependent respiration
Maximal respiration

Figure 4.

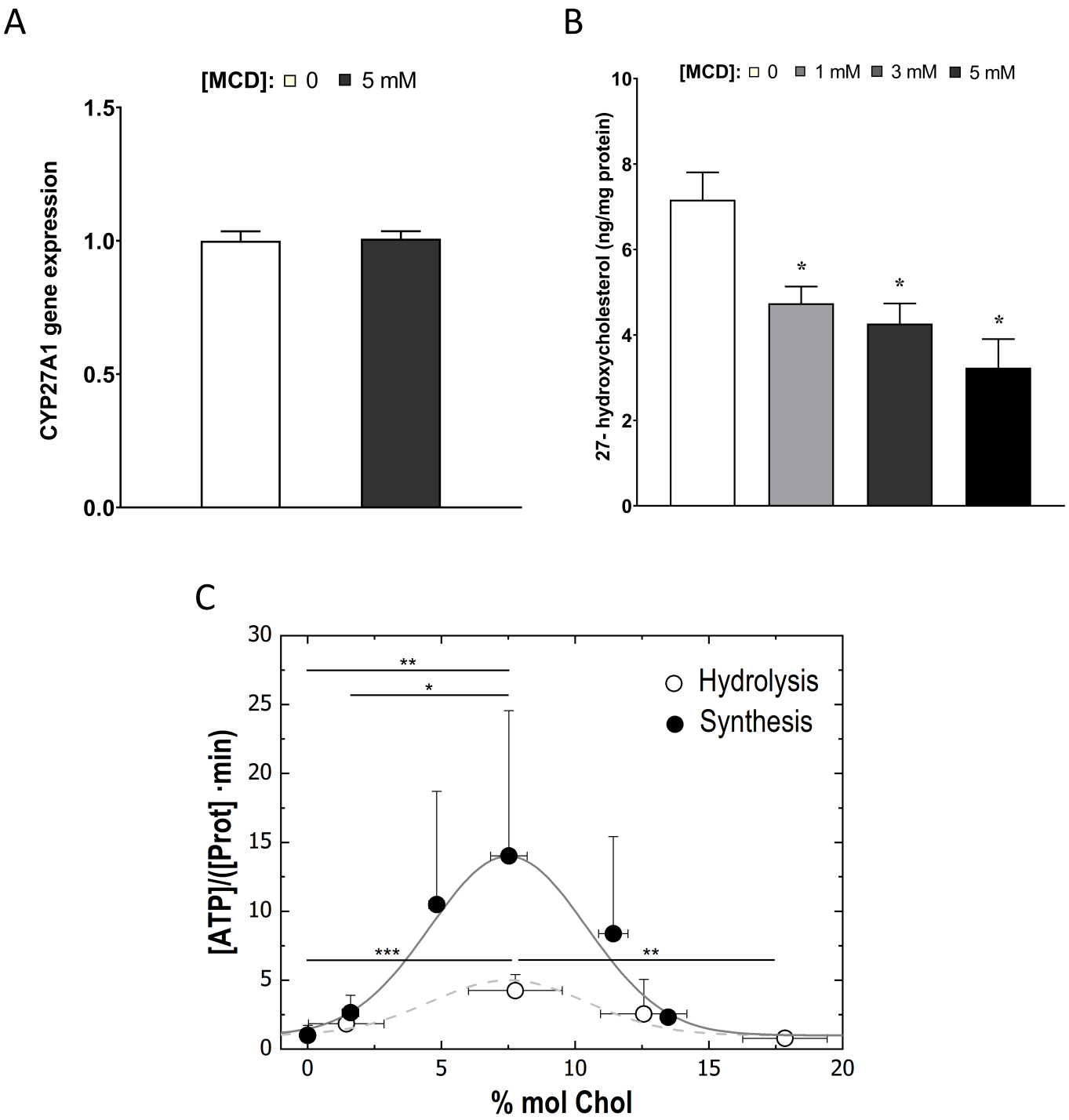
A
[MCD]: 0 5 mM
CYP27A1 gene expression
1.5
1.0
0.5
0.0
B
[MCD]: 0 1 mM 3 mM 5 mM
27- hydroxycholesterol (ng/mg protein)
10
8
6
4
2
0
*
*
*
C
Hydrolysis
Synthesis
[ATP]/([Prot] ·min)
30
25
20
15
10
5
0
**
*
***
**
0
5
10
15
20
% mol Chol

Figure 5.

A

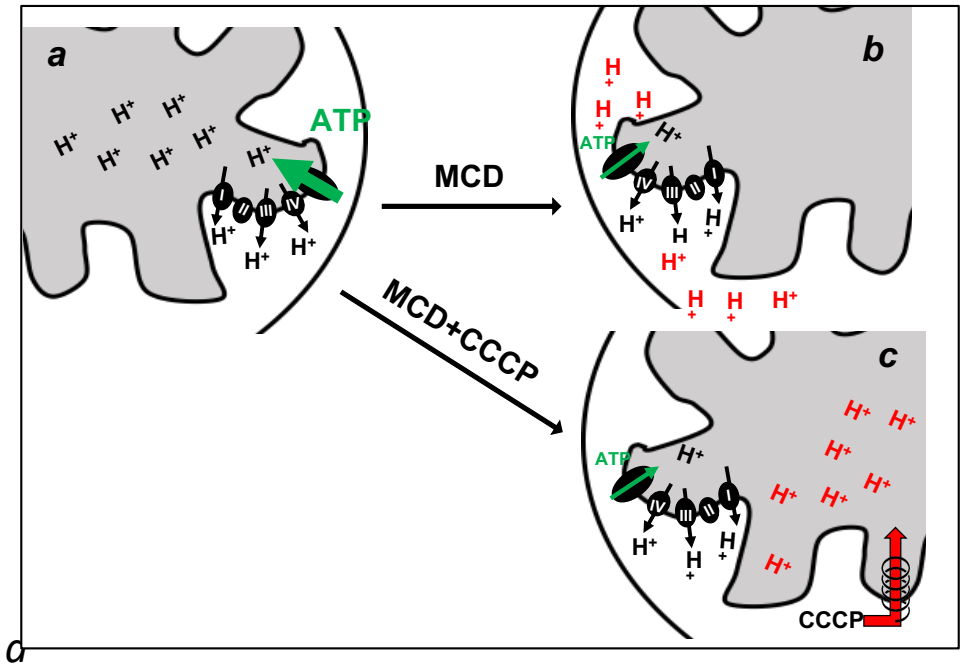
a
ATP
MCD
b
MCD+CCCP
c
CCCP

B

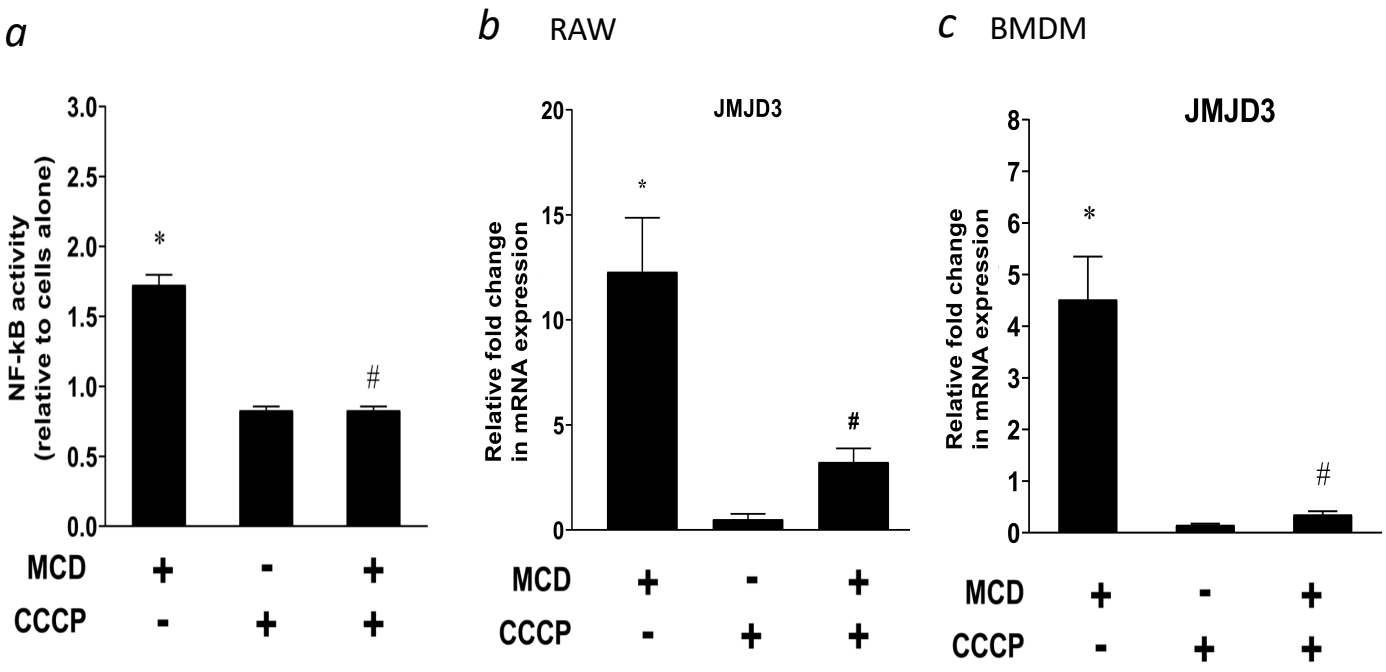
a
NF-kB activity
(relative to cells alone)
MCD + - +
CCCP - + +
b RAW
JMJD3
Relative fold change
in mRNA expression
MCD + - +
CCCP - + +
c BMDM
JMJD3
Relative fold change
in mRNA expression
MCD + - +
CCCP - + +

Figure 5.

B

d

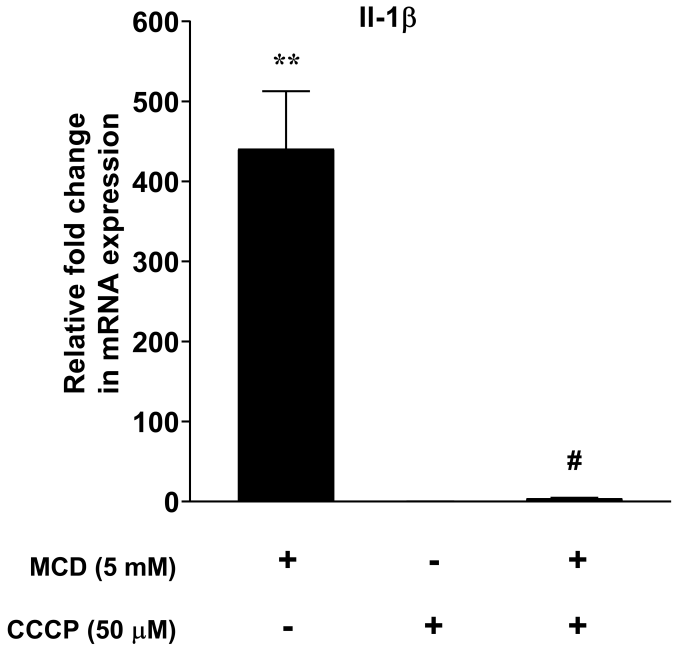
Il-1β
Relative fold change in mRNA expression
600
500
400
300
200
100
0
**
#
MCD (5 mM)
+
-
+
CCCP (50 μM)
-
+
+

Figure 6.

A

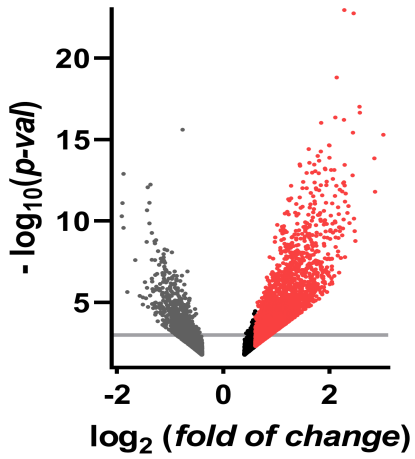

B

a

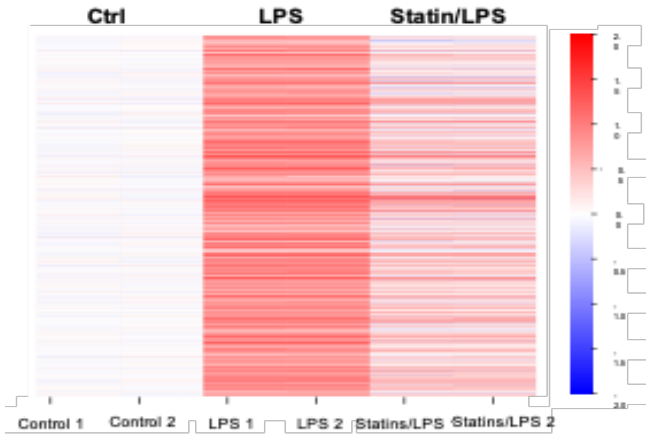

b ***LPS activated genes downregulated by statin***

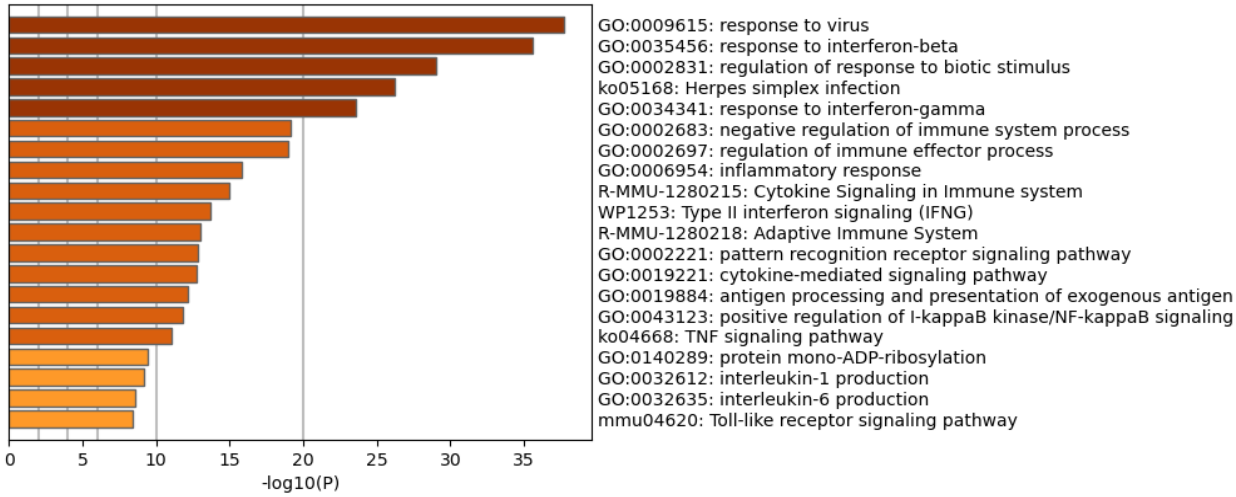

Figure 6.

B

C

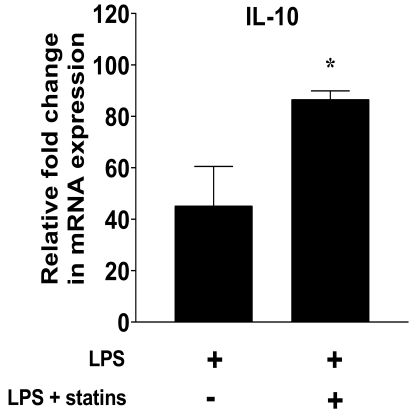
IL-10
Relative fold change in mRNA expression
120
100
80
60
40
20
0
*
LPS
+
+
LPS + statins
-
+

Figure 6

C

a

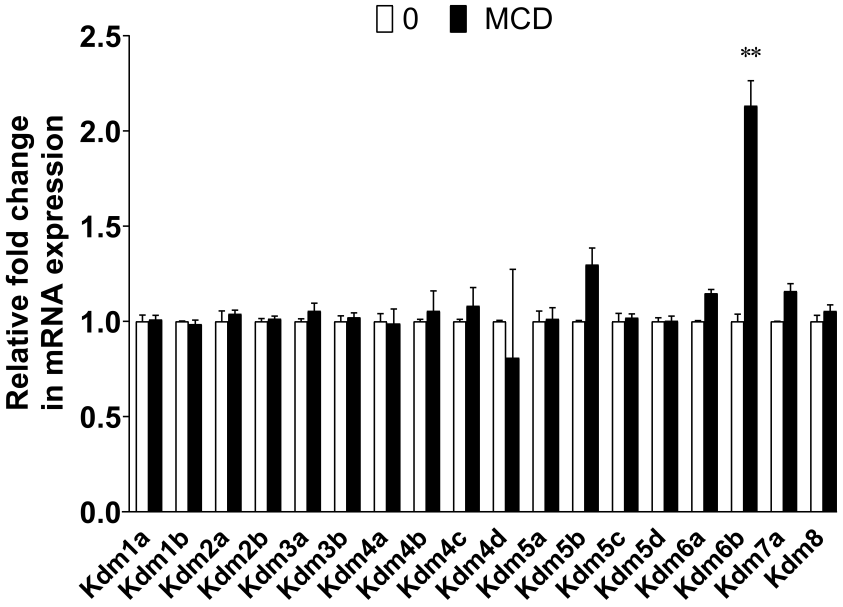

b

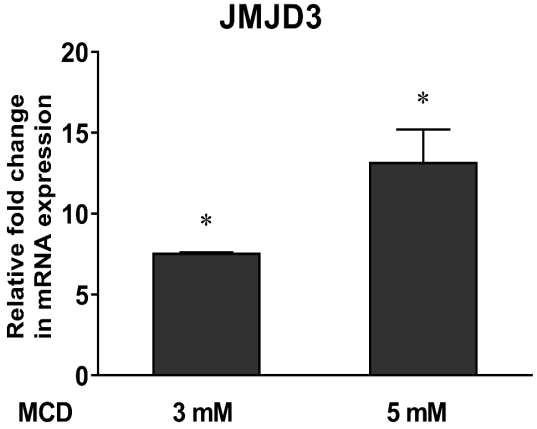

c

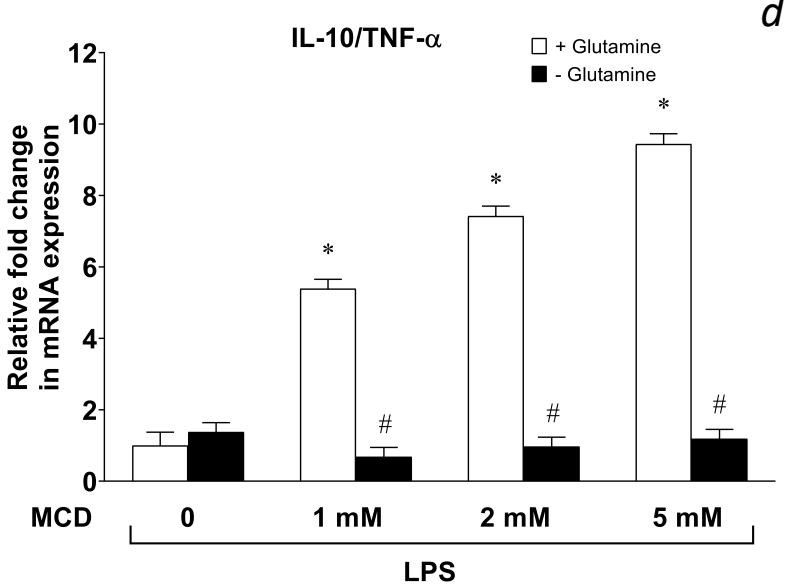

d

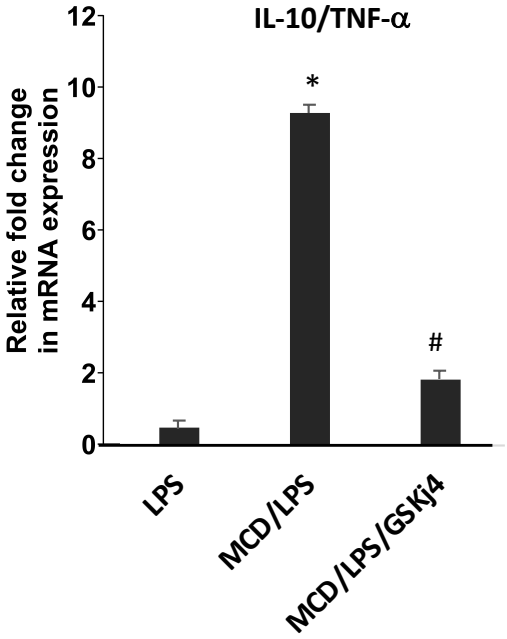

Figure 7

A

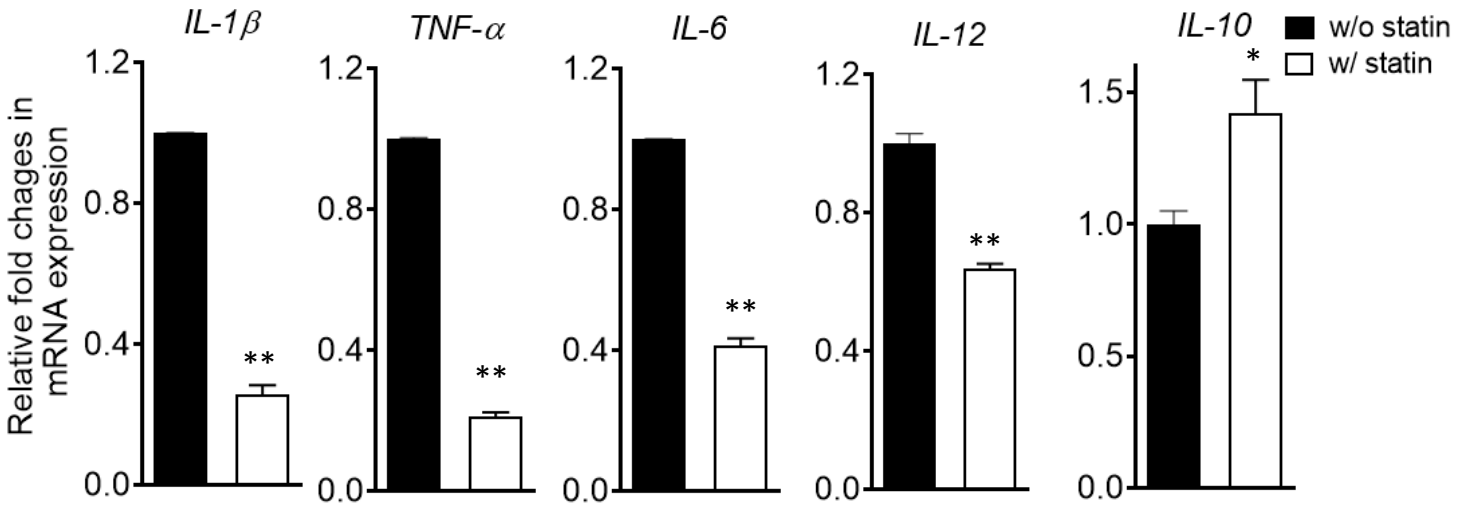

B

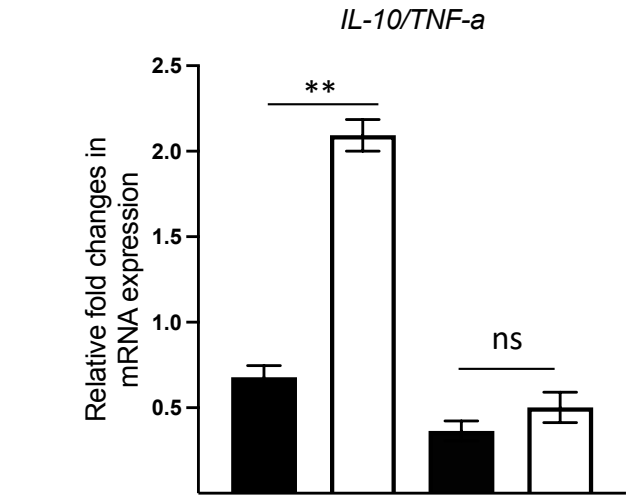

LPS	+	+	+	+
MCD	-	+	-	+
Glutamine	+	+	-	-

Figure 7

C

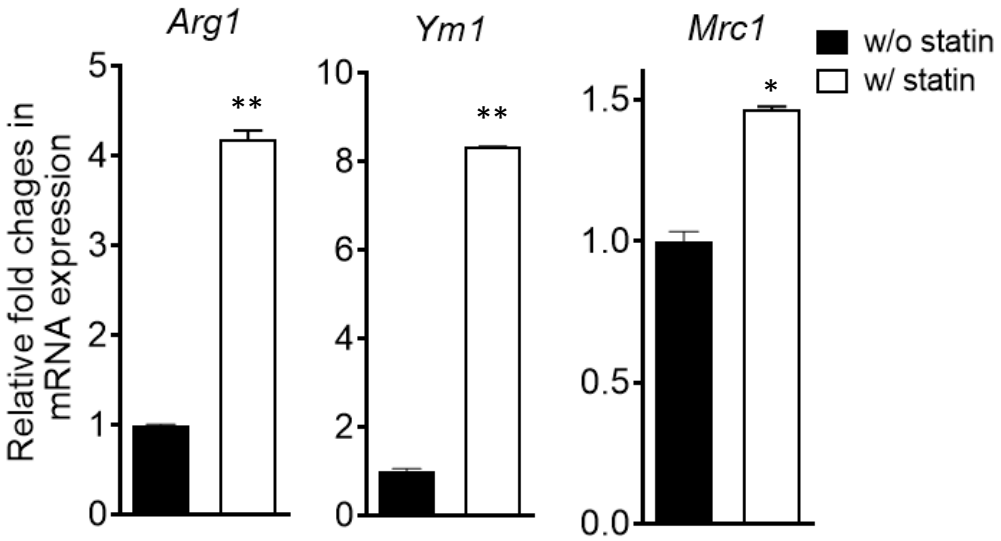
Arg1
Ym1
Mrc1
w/o statin
w/ statin
Relative fold chages in mRNA expression
**
**
*
0
1
2
3
4
5
0
2
4
6
8
10
0.0
0.5
1.0
1.5

D

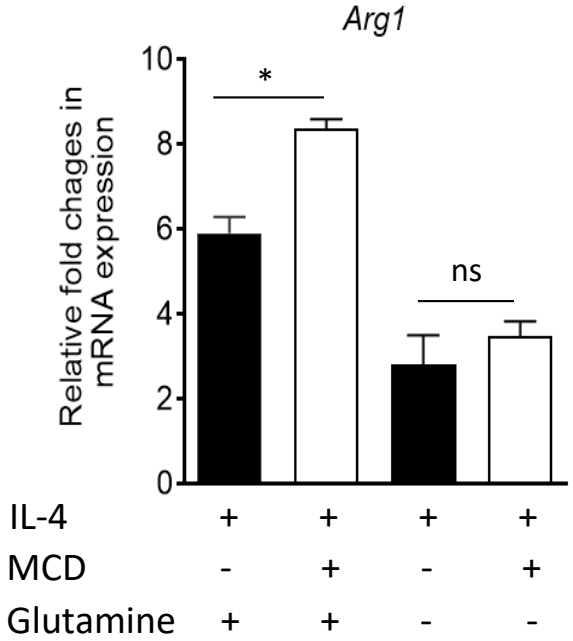
Arg1
Relative fold chages in mRNA expression
*
ns
0
2
4
6
8
10
IL-4 + + + +
MCD - + - +
Glutamine + + - -

Figure 7

E

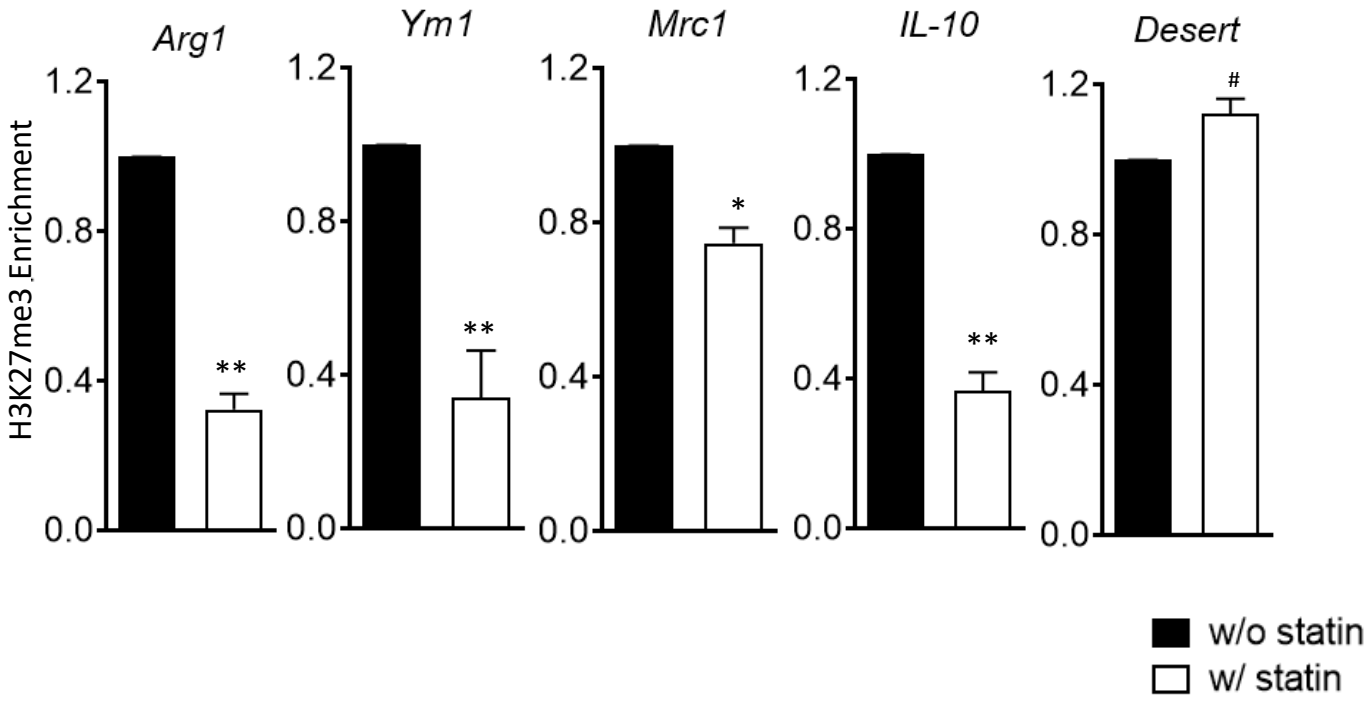
Arg1
Ym1
Mrc1
IL-10
Desert
H3K27me3 Enrichment
1.2
0.8
0.4
0.0
**
**
*
**
#
w/o statin
w/ statin

Supplementary

Figure. 1

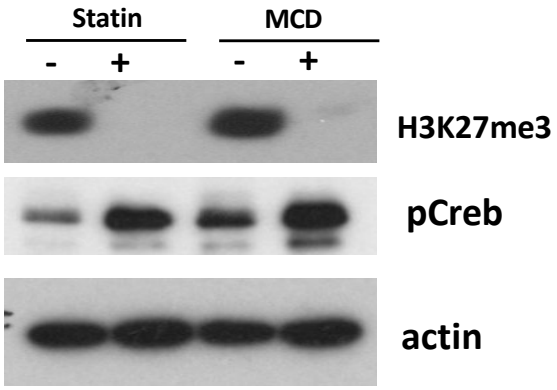

Figure. 2

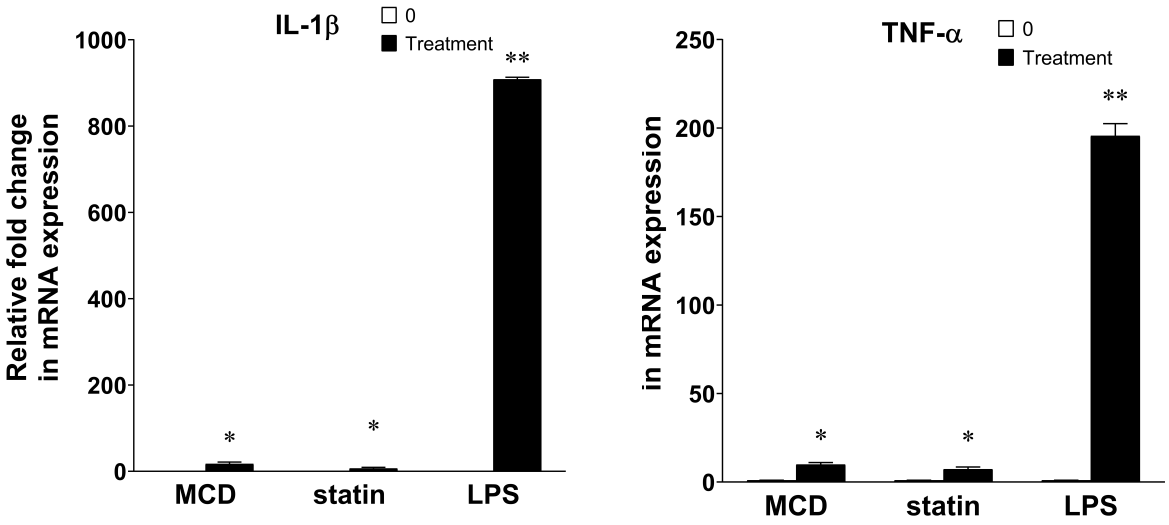

Supplementary

Figure 3.

A

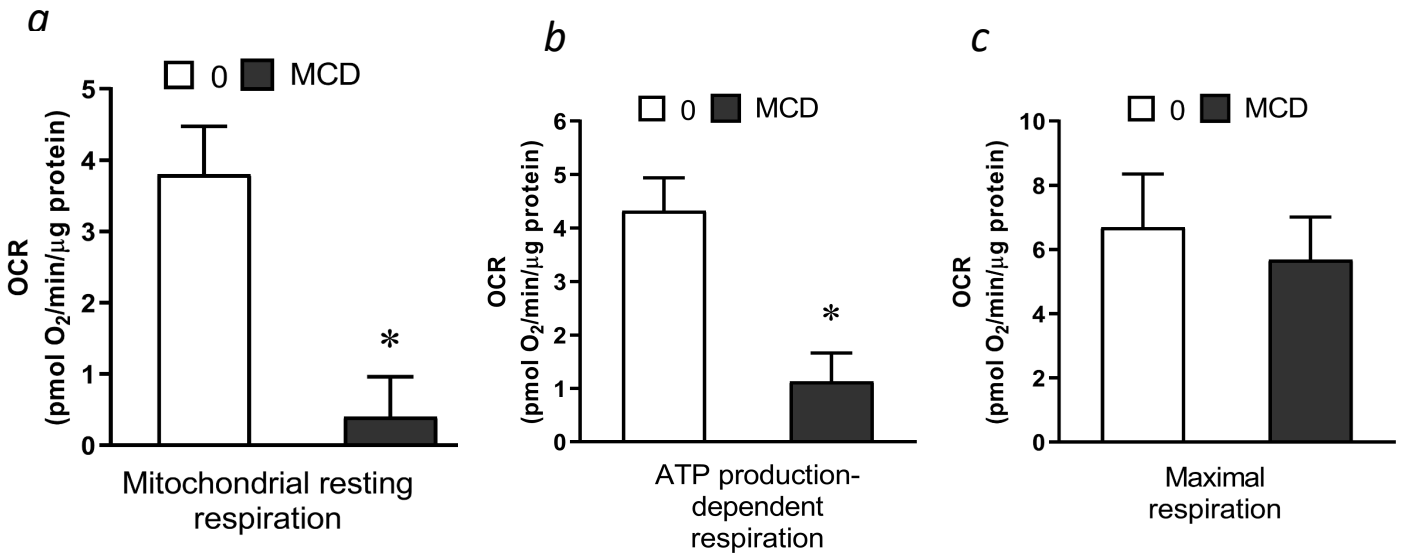

B

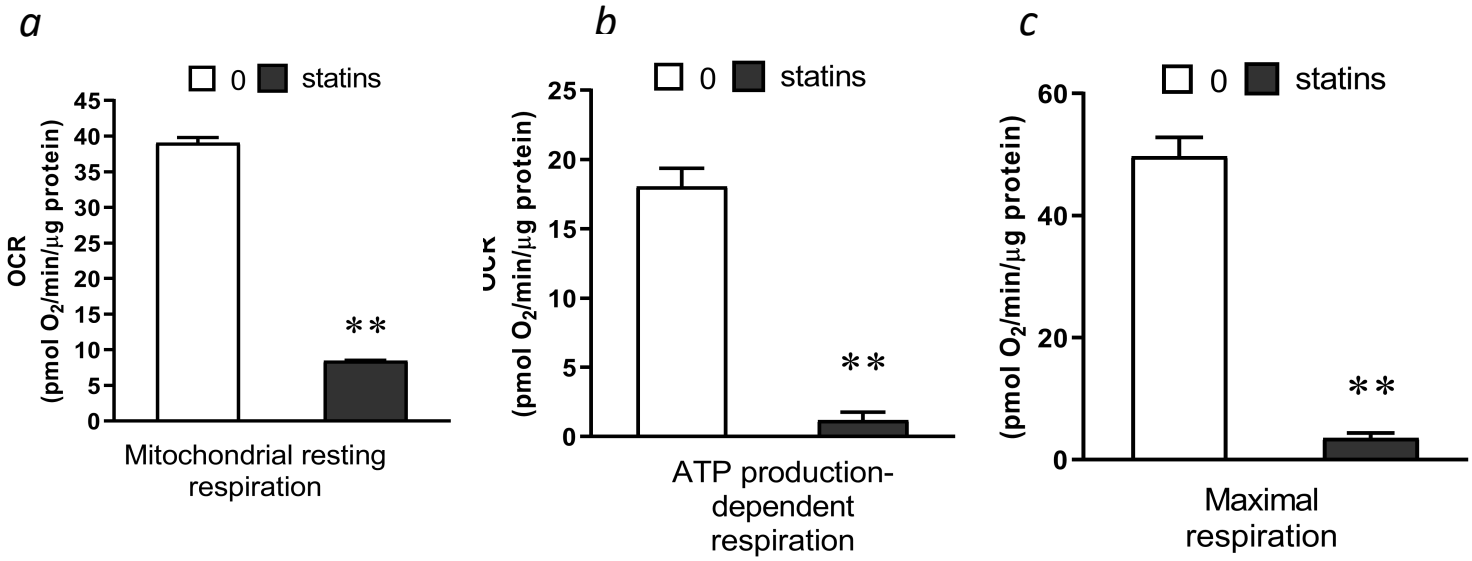

Supplementary

Figure 4

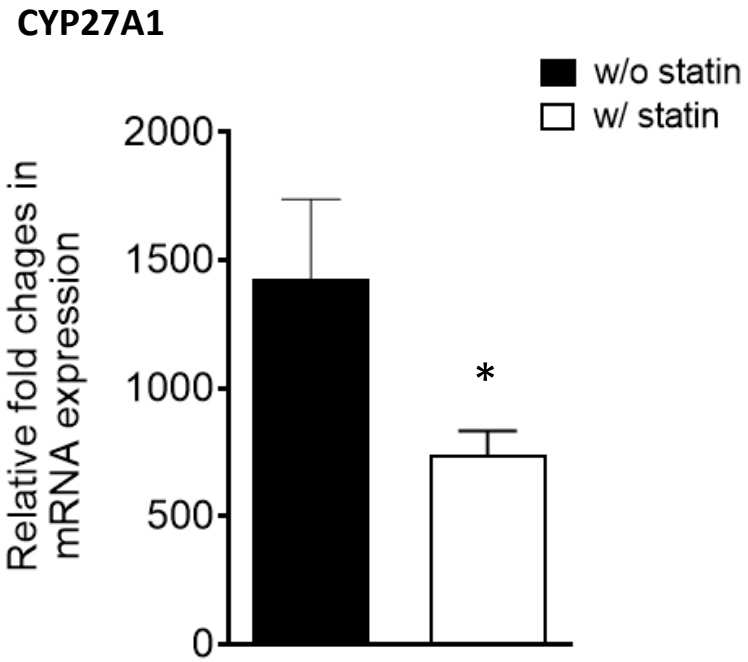

Figure 5

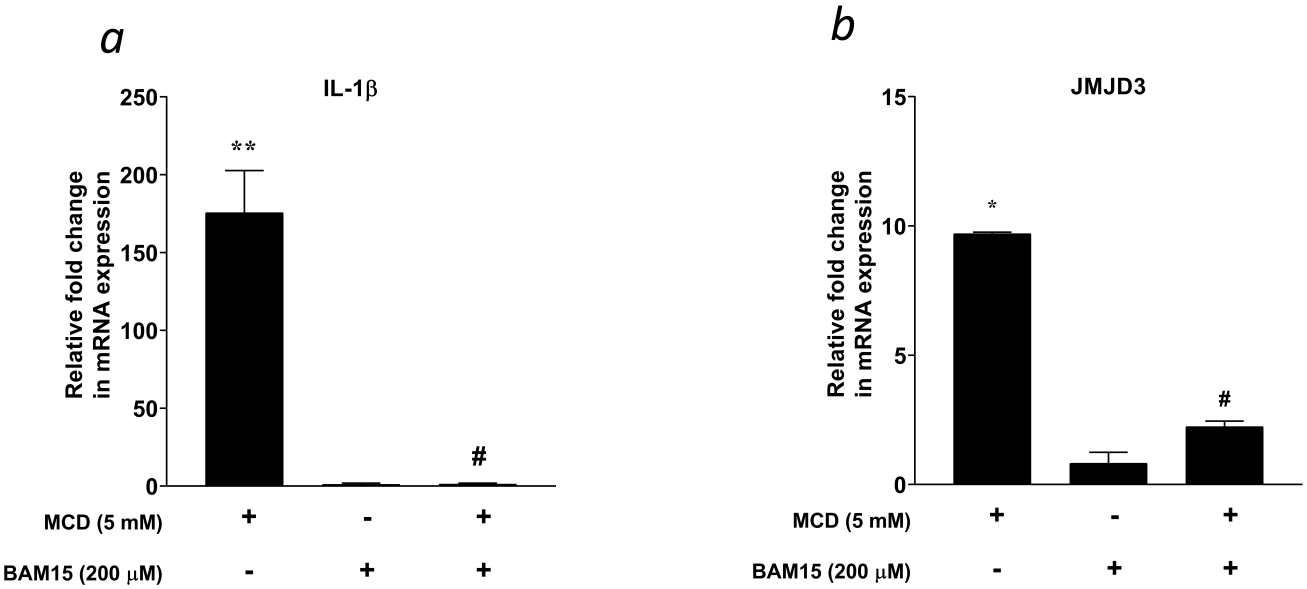

Supplementary

Figure 6.

a

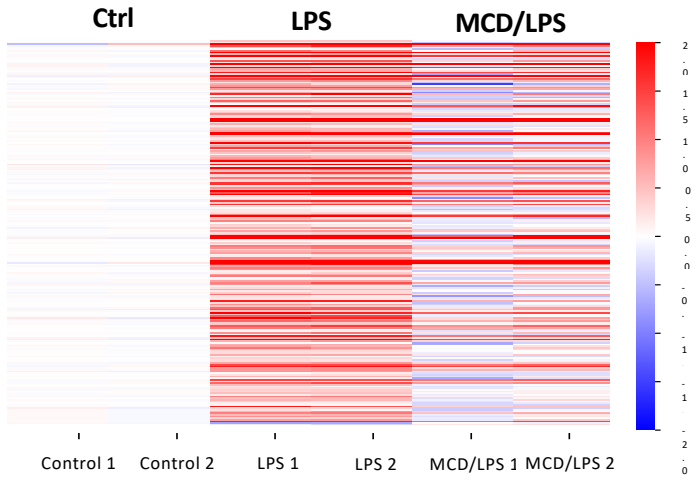

b ***LPS stimulated genes downregulated by MCD***

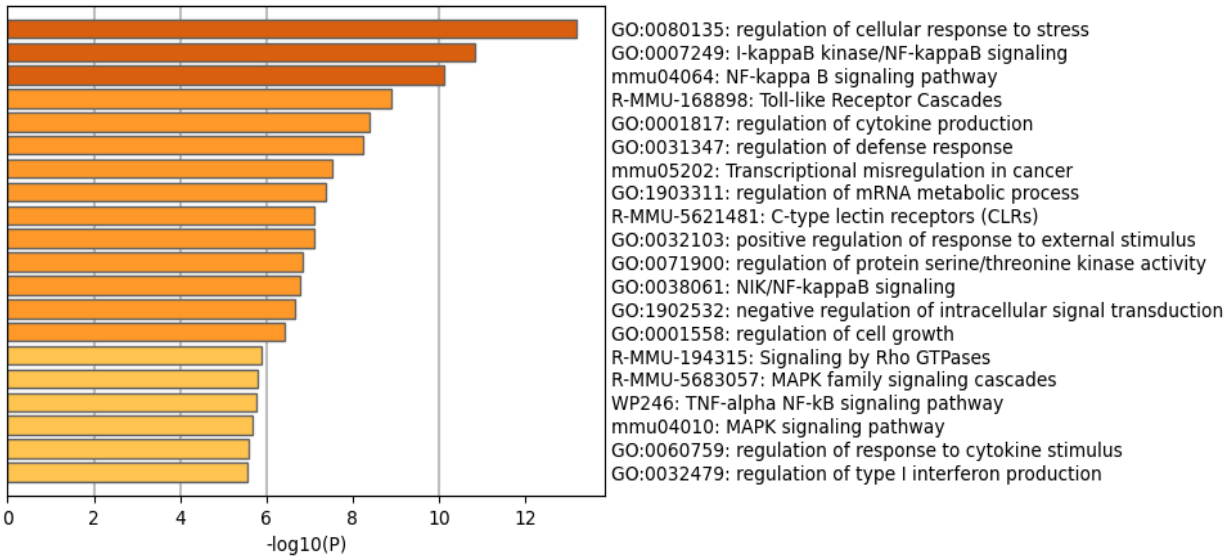

Supplementary
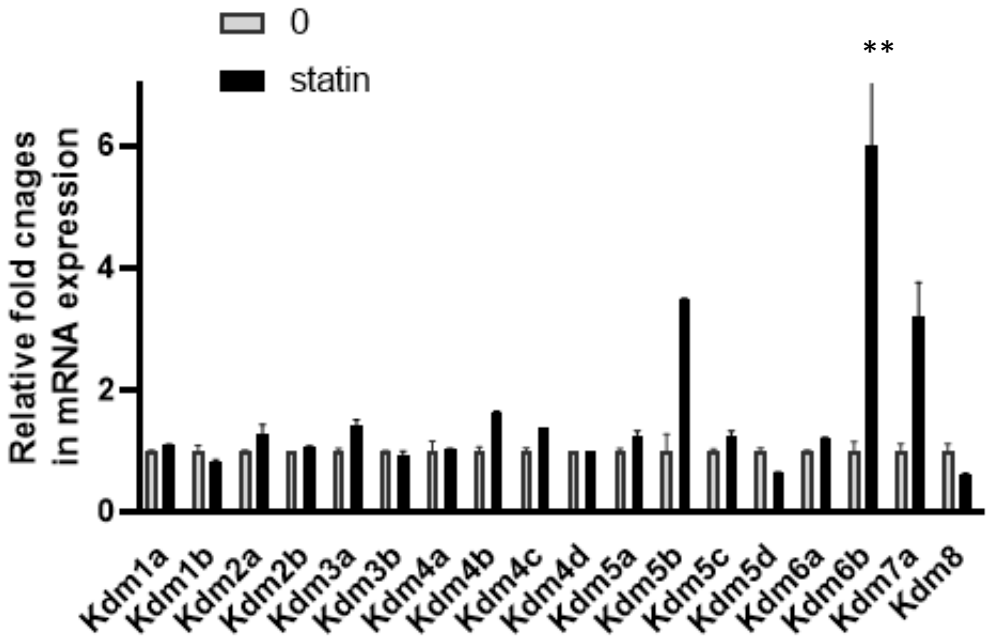
Figure 7.